Politecnico di Torino

POLITECNICO DI TORINO

Master's Degree
in Mathematical Engineering

Master's Thesis

Scattering process from a disklike obstacle of massive vortex pairs in binary BECs

Supervisor
prof. Vittorio Penna

. . . . . .

Candidate
Enrico Ortu

. . . . . .

Academic Year 2023-2024

Abstract

In this work the scattering process of a massive vortex-antivortex dipole from a disklike obstacle has been investigated. The term "massive" [22], [22], [3] refers to the fact that vortices of one species host the atoms of the other species, which thus play the role of massive cores. The motion of massless vortices is described by first-order motion equations, while the inclusion of core mass introduces a second-order time derivative that doubles the number of independent dynamical variables needed and is responsible for a much richer phenomenology. Infact, while complete integrability is reached in the massless case [19] due to the presence of a sufficient number of conserved quantities to ensure such character, the introduction of core masses makes the system not-integrable as the number of degrees of freedom overtakes the number of necessary conserved quantities. The main purpose of this work is then analyzing the dynamical features of a massive pair scattered against a circular obstacle, shedding a light on eventual chaotic behaviour.

The analytical model that will be employed, the so called Point-like model, is of recent development in scientific literature [22], [2] but already proved its accuracy through various comparisons with the well-known Gross-Pitaevskii equations. Recent advances in research [1] showed how, concerning the case of a pair of massless vortices trapped in a circular box, its dynamics is described by a simple precession motion around the trapping center, while the introduction of increasingly bigger core masses leads to the emergence of instabilities [22], [2]. Moreover the absence of tangential entrainment between the fluids composing the cores and the body of vortices has been established, emphasizing how no dissipation should arise in such rotational dynamics. Trapped quantum vortices are also allowed to collide and annihilate when counter-rotating or undergo a coalescence process when corotating [21]

The present work proposes a novel methodology aimed to investigate the behaviour of the vortex pair when interacting with a disk-like obstruction, based on considering its reduction in asymptotic regimes, allowing to identify interesting dynamical sub-regimes.

A mia madre

Se solo potessi
ti donerei i miei anni.
Tu che nascondi dietro i
sorrisi
il dolore
e dietro le rughe gli affanni.
In questo mondo in cui tutti
siamo in ritardo ad amare
tu sempre puntuale.

Contents

Introduction

After an introductory chapter devoted to the phenomenology of ultracold bosons, including Bose-Einstein condensation [8], [16], the emergence of the Superfluid regime [8] as well as the relevance of vortices in scientific literature, the second chapter will contain a brief review of the Gross-Pitaevskii equation in the mean-field limit, together with the hydrodynamic picture [18] of quantum fluids that is extremely advantageous to investigate topological excitations in fluid mediums.

In the third chapter the Point-like model will be derived through the approximation of the usual mean-field Hamiltonian accounting for two-body interactions adopting a flat density profile for the condensate that neglects the presence of vortex singularities. The resulting Hamiltonian of N free vortices will be extended to account for the presence of a circular confining boundary by means of the Virtual Images Method.

The passage to the massive model is performed by introducing a Lagrangian that contains a quadratic kinetic term depending on vortices' masses [2], appropriately justified thanks to the method of the time-dependent variational lagrangian [20] by means of trial quantum-mechanical wavefunctions. The two-component wavefunction, accounting for the presence of biatomic BEC, plugged into the Gross-Pitaevskii Lagrangian functional allows to write Euler-Lagrange equations associated to each time-dependent variational parameter.

In the fourth chapter a different description of the system will be proposed: by making use of the dynamical-algebra approach [19], [4], it is possible to express the model Hamiltonian as a linear combination of generators of a Lie Algebra that allows to find conserved quantities from algebra's invariants. Locating the model in a specific algebraic framework indeed, aside from giving deeper insights in the mathematical characterization of the system by exhibiting the presence of eventual symmetries, permits a more rigorous justification of numerical results by means of deducted conservation laws. A novel result is presented and discussed, showing the surprising existence of dynamical sub-regimes where the role of mass can be

neglected, restoring a much simpler dynamics emobied by the Helmoltz-Kirchoff equations. This result appears to be perfectly compatible with the conserved quantities and confirmed by a vast number of numerical simulations.

In conclusion chapter five contains results from numerical simulations. The resulting motion of the vortex dipole will be analyzed and justified firstly through the consideration of dynamical equations in two asymptotic regimes and then in the light of the algebraic description presented in the previous chapter. The presence of a few conserved quantities infact can conduct to the derivation of a relation between initial velocities and their values long after the influence of the circular obstacle, justifying the existence of a deflection angle after the dipole's interaction with the obstacle.

Chapter 1

Phenomenology of ultracold bosons

"Disorder is simply the order we are not looking for."

Henri Bergson

Bosons are subatomic particles that follow *Bose-Einstein* statistics, characterized by having integer spin (e.g. photons, Higgs boson,..). Unlike fermions, which obey the Pauli exclusion principle, bosons can occupy the same quantum state. At sufficiently low temperatures, bosons can undergo a phase transition known as **Bose-Einstein condensation** where a large fraction of particles condenses into the same quantum state (the lowest energy state), leading to a macroscopic quantum phenomena.

Such groundbreaking phenomenon was originally proposed on the theoretical level by Satyendra Nath Bose and Albert Einstein in the early 1920s, predicting that below a critical temperature, a dilute gas of bosons would exhibit an exotic collective behaviour. Experimental observations arrived only in the mid-1990s when advancements in cooling and trapping techniques made it possible to achieve BECs in dilute atomic gases.

At low temperatures, bosons can also be observed in the state of **superfluid**. Originally discovered in the 1930s, superfluid state was first observed in helium-4 and it is characterized by the complete absence of viscosity allowing the fluid to flow without dissipation. As properly emphasized in the following, Superfluidity and BEC can co-occur in the same system but the two states are not synonyms of the same spectrum of phenomena.

1.1 Bose-Einstein Condensation

The condensation phenomena [16] interests *spinless* quantum particles at low temperatures. Contrary to classical ones, quantum particles are *indistinguishable* since over a lenghtscale comparable to the de Broglie wavelenght, Heisenberg's uncertainty principle emphasizes the intrinsic indetermination that characterizes the quantum realm. Through the method of the *most probable distribution* [18] within the theory of Grand Canonical Ensemble, typycally adopted when dealing with large systems made up of a fluctuating number of particles, it is possible to find the partition function that describes the system. More specifically, owing to its symmetrical character, bosons are described by the following

$$\mathcal{Z}_B = \prod_p \left[\frac{1}{1 - ze^{-\beta\epsilon_p}} \right]$$

where $\epsilon_p = p^2/2m$ and index p comes from the enumeration of all possible momenta that particles may possess, meaning that $\vec{p} = \hbar\vec{k}$, with wavevector $\vec{k} = 2\pi/L(n_x, n_y, n_z)$ and $n_i \in \mathbb{Z}$. This implies then that momenta of particles assume discrete values. Parameters μ and $z = e^{\beta\mu}$ respectively stands for the chemical potential and the fugacity. The Bose-Einstein distribution function describes then the distribution of bosons over energy E as

$$f_{BE}(E) = \frac{1}{e^{(E-\mu)/k_BT} - 1}$$

where given E_0 the lowest energy level, it is required that $\mu \leq E_0$. Reasonably, BE statistics reproduces Boltzmann's distribution for classical particles for $(E - \mu)/k_BT \gg 1$ (i.e. in the classical limit, for high energies E).

The average occupancy of the $p - th$ energy level is given by

$$\langle n_p \rangle = \frac{ze^{-\beta\epsilon_p}}{1 - ze^{-\beta\epsilon_p}}$$

which presents an accumulation of particles in state $p = 0$ for $E \to \mu^+$. For mathematical convenience a passage to a continuum description is typically addressed by replacing previous variables with continuous quantities, allowing to recast the number of particles at energy E by means of the function

$$N(E) = f_{BE}(E)g(E) = \frac{1}{e^{(E-\mu)/k_BT} - 1} \frac{2\pi(2m)^{\frac{3}{2}}\mathcal{V}}{h^3} \sqrt{E} \sim \frac{\sqrt{E}}{e^{(E-\mu)/k_BT} - 1}$$

where $g(E)$ is the density of states in the continuous picture for an ideal gas confined in a box of volume $\mathcal{V}$.

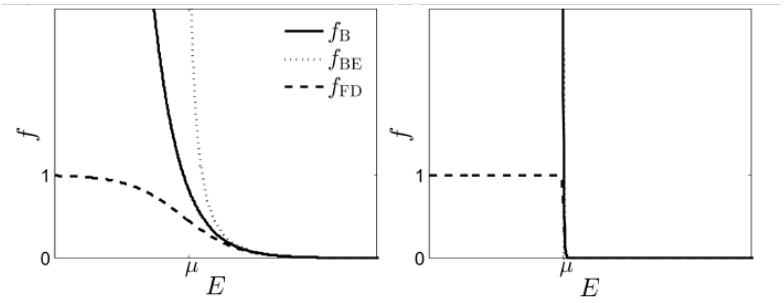

Figure 1.1: The Boltzmann, Bose-Einstein and Fermi-Dirac distribution functions for $T \gg 0$ on the left, for $T \approx 0$ on the right

As shown in the following picture [8], the occupancy of the energy levels $N(E)$ goes to zero for $E \to 0$ due to the diminishing density of states in this limit, while the occupancy of a state (corresponding instead to $f_{BE}(E)$) diverges as $E \to \mu$. Exploiting the passage to the continuous picture leads to recast the occupancy of

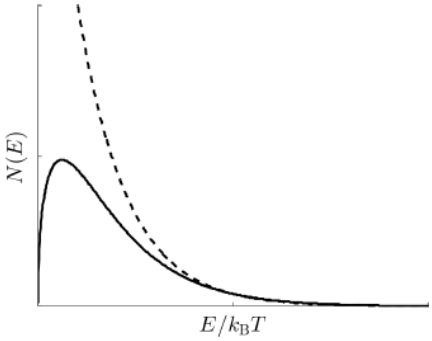

Figure 1.2: Solid line represents the occupation of energy levels, while the dashed line stands for the occupation of energy states

energy levels by means of the Riemann zeta function as

$$N = \frac{(2\pi m k_B T)^{\frac{3}{2}} \mathcal{V}}{h^3} g_{3/2}(z)$$

a formulation that more advantageously permits to predict the emergence of Bose-Einstein Condensation. Indeed function $g_\beta(z)$ has the form

$$g_\beta(z) = \sum_{p=1}^{+\infty} \frac{z^p}{p^\beta} \overset{z=1}{\to} \zeta(\beta) = \sum_{p=1}^{+\infty} \frac{1}{p^\beta}$$

and $g_{3/2}(z)$ is bounded from above reaching its maximum value for $\zeta(3/2) \approx 2{,}612$ (for $z = 1$). The system becomes then *saturated with particles* with a **critical number** N_c. More precisely, this indicates the saturation of the excited states meaning that any additional particle added to the system (beyond N_c) enters (at zero energy cost) the *ground state* that acquires an incredibly large population.

Considering the case of fixed particle number instead, the condensation phenomena can be observed when crossing a specific **critical temperature** T_c: for temperatures beyond such value condensation occurs, otherwise the gas is in the normal phase. Such critical value is given by

$$T_c = \frac{h^2}{2\pi m k_B}\left[\frac{N}{\zeta(3/2)\mathcal{V}}\right]^{\frac{3}{2}}$$

directly linked to the **condensate fraction** $\langle n_0\rangle/N$ describing the proportion of condensed particle

$$\frac{\langle n_0\rangle}{N} = 1 - \left(\frac{T}{T_c}\right)^{\frac{3}{2}}$$

It is important to remark that such low-temperatures collective phenomena refers to a condensation in *momentum space* (and not in real physical space) with $p = 0$ and can be outlined as follows:

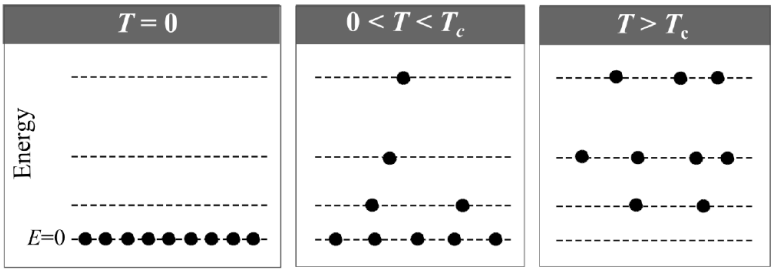

Figure 1.3: Illustration of the macroscopic occupation of quantum state $p = 0$: for $T = 0$ the fraction of condensed particles is maximum, while it decreases for $T > 0$ as higher energy levels become populated

By investigating the behaviour of the *heat capacity* c_V (the amount of energy required to raise the temperature by a unit amount at constant volume) it becomes possible to emphasize an important aspect. By means of thermodynamical considerations based on the derivation of a suitable equation of state, it is possible to show that the behaviour of $c_V(T/T_c)$ when crossing the critical value $T/T_c = 1$ is

subject to a drastic change. Indeed:

$$c_V \begin{cases} \sim T^{3/2} & \text{if } T < T_c \\ = C & \text{if } T \gg T_c \end{cases} \tag{1.1}$$

the presence of discontinuities in the first derivative of c_V is the sign of **critical behaviour** meaning that a transition between two distinct states of matter is occurring. As appropriately discussed in the following section, a strong analogy

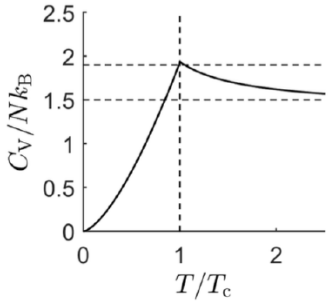

Figure 1.4: Heat capacity as a function of critical parameter T/T_c

is noticed in the behaviour of the heat capacity of liquid Helium that similarly exhibit critical behaviour.

1.2 Superfluidity

The exploration of low temperatures began in 1820s, where experimental chemists discovered a way to liquefying chlorine at a temperature of $239K$. Later on nitrogen and hydrogen followed until, in the early 1900s H. K. Onnes succeded in the liquefaction of helium ^{4}He, reaching an extraordinary temperature of $4K$, worth a Nobel Prize in Physics. The first observation was the absence of resistance below $4K$, then at around $2{,}2K$ its heat capacity undergoes a discontinuous change, leading to postulate the the existence of two distinct phases of liquid helium: helium-I above a certain critical temperature T_λ and helium-II below. Moreover helium-II showed to remain liquid even for $T \to 0$ and together with other experimental observations, its phase diagram started to differ from a conventional fluid. In 1930s it was suggested that the condensation phenomena theorized by Einstein and Bose could have been useful to explain *superfluid* behaviour. However Bose-Einstein condensation was meant to describe an ideal (quantum) gas with no (or negligible) interactions, predicting the emergence of a macroscopic collective behaviour [8]. The strong similarity in the discontinuity appearing in the plot of the heat

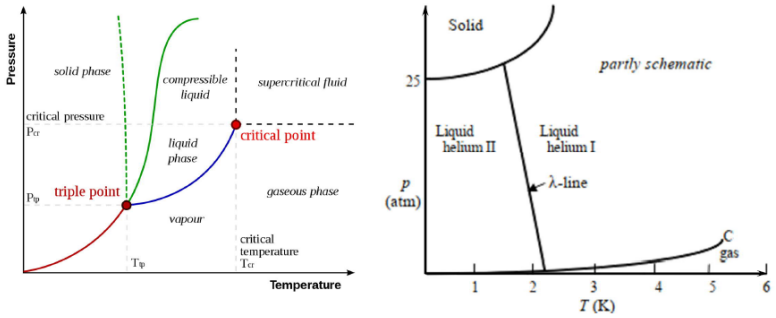

Figure 1.5: Comparison between the phase diagram of helium and a conventional fluid. An important difference lays in the lack of a triple point.

capacity infact led to develop a two-fluid model by Lev Landau, that considered helium-II as a combination of a viscosity-free fluid and a conventional viscous one.

Later on the discovery that composite electrons forming *Cooper pairs* could un-

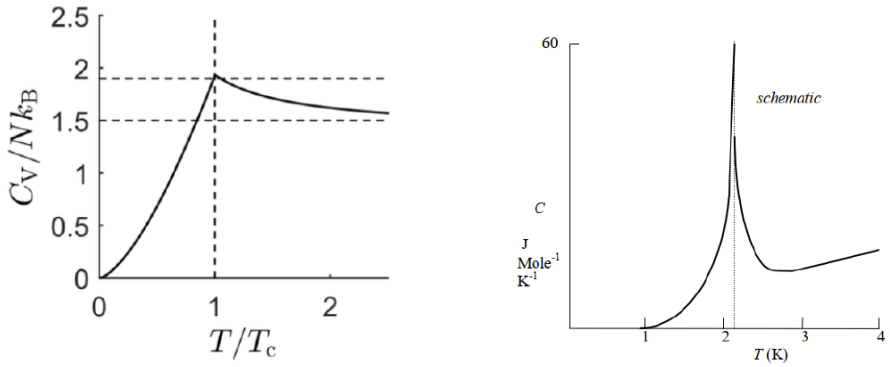

Figure 1.6: Comparison between the heat capacity c_V of a BEC (left) and liquid helium (right).

dergo a condensation phenomena allowed to observe superfluidity in the fermionic isotope ^{3}He showing the possibility to exploit condensation. In this regard then, superfluids and superconductors (regarded as fluids made of charged Cooper pairs) can be seen as manifestations of Bose-Einstein condensation. It is important to stress the fact that despite helium superfluid exhibits some BEC properties the two states are not identical: while at $T = 0$ BEC prescribes the macroscopic occupation of the lowest energy quantum state, liquid helium may possess particles laying at higher energy levels. Indeed condensation is a phenomena that has been theorized in an ideal quantum gas (i.e. not interacting) while the presence of not-negligible

interactions in quantum fluids and superconductors addresses major complications.

Superfluid ^{4}He [9] can flow without friction through pipes, extremely narrow channels where conventional fluids would be governed by viscosity, but it also presents a critical velocity above which superflow breaks down and most importantly **quantized vortices** to which is devoted this work.

1.3 The emergence of vortices in ultracold bosons and BECs

The study of quantum vortices in superfluids began in 1950s when Richard Feynman published a groundbreaking article regarding the properties of liquid Helium. The observation of topological excitations in such fluids indeed was a proof of superfluid character [9], marked by the emergence of a microscopic order. Indeed, superfluid state is characterized by the macroscopic occupation of a quantum state resembling the condensation phenomena, resulting in a collective phase coherence.

The creation of a Bose-Einstein condensate in dilute trapped ultracold atomic gases led to the discovery of a new possible superfluid medium that, from the experimental viewpoint, possesses many technical advantages. The dilute-gas BECs [11] indeed differ from superfluid ^{4}He since the GPE provides a remarkably detailed description, allowing a careful comparison of theory and experiment. Moreover the investigation of bosonic mixtures of BECs [12], [3] allowed to observed quantized vortices profoundly different from the one typically present in single-component BECs. As a consequence of a peculiar interplay between repulsive inter-species and intra-species interactions, one of the two components can be confined in the vortex cores of the other component, leading to a complete phase separation. Such configuration, the *immiscibility regime*, arises for sufficiently intense inter-species interactions where the cores correspond to density peaks of the other species and viceversa. On the pratical level a finite repulsive coupling causes a slight compenetration of the two due to the centrifugal force acting on the internal species. This results in a light mismatch between peaks and singularities as depicted in figure 1.7. Internal species play the role massive cores providing an inertial (kinetic) contribution in the dynamics requiring a more general approach based on the introduction of a customized Lagrangian.

Being the dynamics ruled by a non-linear Schrödinger equation (GPE), one typically refers to soliton solutions, particular non-linear waves that emerge in the 1D case. Solitons can be seen as localized excitations which, because of the competition between dispersion and non-linear effects, propagate keeping their

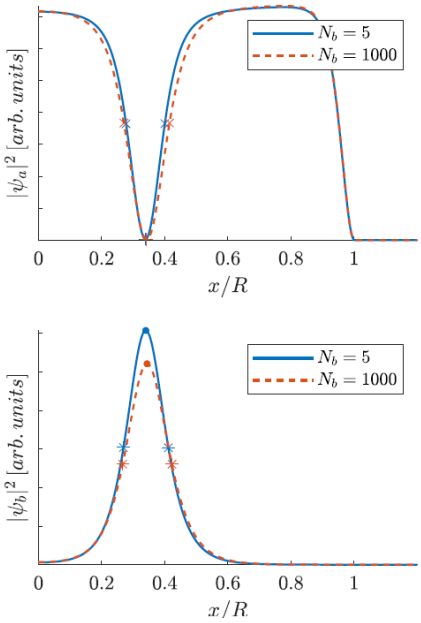

Figure 1.7: Density profiles of the two involved species: the peaks of b-species (core) correspond to singularities of a-species (vortex body.

shape unaltered. Depending on the sign of the interaction parameter, either *dark* or *bright* solitons are possible. Despite the problem under investigation is not one-dimensional, the profiles of the vortex core and body can be described by wavefunctions possessing soliton properties, typically addressed as solitary waves. Nevertheless in binary mixtures symbiotic solitons emerge as a consequence of the interplay between attractive and repulsive forces between the components, resulting in structures addressed under the name of *vortex-bright soliton complexes* [22].

Chapter 2

Mathematical formalism of Quantum Fluids

"Mathematics is the art of giving
the same name to different things."

Henri Poincarè

This section is devoted to the presentation of the essential mathematical aspects employed in the description of ultracold bosons. Firstly the *Weakly interacting Bose Gas* will be presented together with a brief description of the Bogoliubov approximation scheme and the derivation of a fundamental equation in the *Mean-Field Limit*: the **Gross-Pitaevskii Equation**.

The second part of this chapter focuses on the emergence of *vortex states*: first from a topological perspective by rearranging the GPE in the **Hydrodynamic Picture** exploiting the deep connection between quantum fluids and classical ones. Subsequently vortices will be seen from a thermodynamical point of view analyzing the Bose Gas in low-dimensions and discussing the renowned *Berezinskii-Kosterlitz-Thouless* phase transition.

2.1 GPE in Mean-Field limit

Considering a system made up of N-bosons under the hypotesis of **dilute gas** and below the **critical temperature** the **Bogoliubov approximation scheme** [16], [18] allows to find important information relative to the energy spectrum of the system under investigation.

Within the second-quantization picture, the Hamiltonian describing a Bose gas with interactions modeled for a two-body interaction potential $U(\vec{r})$ reads:

$$\mathcal{H} = \int d^2x \psi^\dagger(x,t) H_0(x) \psi(x,t) + \frac{1}{2} \int d^3x \int d^3s \psi^\dagger(x,t)\psi^\dagger(s,t) U(|x-s|)\psi(x,t)\psi(s,t) \tag{2.1}$$

where $H_0 = -\frac{\hbar^2}{2m}\nabla^2 + V(\vec{r})$ and typically $U(|\vec{r}-\vec{s}|) = U_0\delta^3(\vec{r}-\vec{s})$.

While in absence of a trapping potential it is possible to exploit the harmonic-oscillator basis $\{\phi_\alpha(\vec{r})\}$ and represent the quantized field in terms of superposition of plane-waves, when the system is actually confined in a box a more general representation of the field ψ is necessary. The **Generalized Bogoliubov approach** suggest to express the field in terms of a set of unknown modes $A_l(t)$ and basis $\{f_l(\vec{r})\}$:

$$\psi(x,t) = \sum_l A_l(t) f_l(\vec{r}) = \Phi(\vec{r},t) + \sum_{l\neq 0} A_l(t) f_l(\vec{r}) = \Phi(\vec{r},t) + \Delta\psi(\vec{r},t) \tag{2.2}$$

differentiating the term corresponding to the ground state $\Phi(\vec{r},t) = A_0(t) f_0(\vec{r})$ (where as a consequence of Bogoliubov approximation scheme $[A_0, A_0^\dagger] \simeq 0$ and so A_0 is a scalar quantity) and the one concerning weakly occupied modes $\Delta\psi$. In such setting the statistical average of operator $\Delta\psi(\vec{r},t)$, accounting for both thermal and quantum fluctuations, approaches zero at $T = 0$, suggesting that quantum fluctuations become negligible in the thermodynamic limit. Thus considering the non-linear Schröedinger equation arising from the mean-field Hamiltonian (2.1) and its expectation value from both sides:

$$i\hbar\partial_t \langle\psi(\vec{r},t)\rangle = H_0(\vec{r})\langle\psi(\vec{r},t)\rangle + U_0\langle\psi^\dagger(\vec{r},t)\psi^2(\vec{r},t)\rangle \tag{2.3}$$

by means of eq. (2.2) and of the **Mean-field approximation** for operator products, one obtains the **Gross-Pitaevskii equation**:

$$i\hbar\partial_t \Phi(\vec{r},t) = H_0(\vec{r})\Phi(\vec{r},t) + U_0|\Phi(\vec{r},t)|^2\Phi(\vec{r},t) \tag{2.4}$$

describing the dynamical evolution of field $\Phi(\vec{r},t)$, the system's order parameter: the lowest energy quantum state is *macroscopically occupied* by a large number of bosons.

2.2 Hydrodynamic picture and Topological Excitations

The passage to the Hydrodynamic picture [18] provides an advantageous framework in which reformulating the GPE, as well as exploit the emergence of single and multi-vortex configurations in the fluid medium.

Starting from the Mean-Field Hamiltonian (2.1) we here recall that field ψ plays the role of an *order parameter* describing the numerical density of particles, since $N = \int d^2\vec{r}|\psi|^2$. Obeying to classical (field) Poisson Brackets $\{\psi(\vec{r}), \psi^*(\vec{s})\} = \delta^2(\vec{r}-\vec{s})/i\hbar$, the resulting dynamics is ruled by *non-linear Schröedinger equations* of the form:

$$\begin{cases} i\hbar\dot{\psi} &= \frac{\hbar^2}{2m}\nabla^2\psi + V(\vec{r})\psi + U|\psi|^2\psi \\ i\hbar\dot{\psi^*} &= \frac{\hbar^2}{2m}\nabla^2\psi^* - V(\vec{r})\psi^* - U|\psi|^2\psi^* \end{cases} \tag{2.5}$$

Introducing new fields ρ, θ linked to ψ by means of field transformations

$$\psi, \psi^* \mapsto \rho \doteq |\psi|^2, \quad \theta \doteq \frac{1}{2i} ln\left(\frac{\psi}{\psi^*}\right)$$

it is first possible to prove that their PB are still canonical (meaning that $\{\rho(\vec{r}), \theta(\vec{s})\} = 1/\hbar\delta^2(\vec{r}-\vec{s})$) observing that $\psi = \sqrt{\rho}e^{i\theta}$. At this point it is possible to plug fields ρ and θ inside the mean-field Hamiltonian:

$$\begin{aligned} \mathcal{H} &= \int d^2\vec{r}\left[-\frac{\hbar^2}{2m}|\nabla\psi|^2 + V(\vec{r})|\psi|^2 + \frac{U}{2}|\psi|^4\right] \\ &= \int d^2\vec{r}\left[\frac{\hbar^2}{2m}\left(\frac{1}{4\rho}(\nabla\rho)^2 + \rho(\nabla\theta)^2\right) + V(\vec{r})\rho + \frac{U}{2}\rho^2\right] \end{aligned} \tag{2.6}$$

due to relations

$$\nabla\psi = \nabla\left(\sqrt{\rho}e^{i\theta}\right) = e^{i\theta}\left(\frac{\nabla\rho}{2\sqrt{\rho}} + \sqrt{\rho}i\nabla\theta\right)$$

and

$$|\psi|^2 = \frac{1}{4\rho}(\nabla\rho)^2 + \rho(\nabla\theta)^2$$

Dynamical equations are calculated as follows, for field ρ:

$$\begin{aligned} \dot{\rho} = \{\rho, \mathcal{H}\} &= \frac{1}{\hbar}\frac{\delta\mathcal{H}}{\delta\theta} = \frac{1}{\hbar}\int d^2\vec{r}\left[\frac{\hbar^2}{2m}2\rho\nabla\theta\cdot\nabla\frac{\delta\theta(\vec{r})}{\delta\theta(\vec{x})}\right] \\ &= \frac{1}{\hbar}\int d^2\vec{r}\left[\frac{\hbar^2}{2m}\mathrm{div}\left(\rho\nabla\theta\delta^2(\tilde{\mathrm{r}}-\tilde{\mathrm{x}})\right) - \delta^2(\tilde{\mathrm{r}}-\tilde{\mathrm{x}})\mathrm{div}(\rho\nabla\theta)\right] \\ &= -\frac{\hbar}{2m}\int d^2\vec{r}\,\mathrm{div}(\rho\nabla\theta)\delta^2(\tilde{\mathrm{r}}-\tilde{\mathrm{x}}) = -\frac{\hbar}{2\mathrm{m}}\nabla(\rho\nabla\theta) \end{aligned} \tag{2.7}$$

where in last line Green-Gauss formula has been employed to assure that

$$\int d^2\vec{r}\mathrm{div}\big(\rho\nabla\theta\delta^2(\tilde{\mathrm{r}}-\tilde{\mathrm{x}})\big)=0$$

Similarly for field θ:

$$\begin{aligned}\dot{\theta}=\{\theta,\mathcal{H}\}&=-\frac{1}{\hbar}\frac{\delta\mathcal{H}}{\delta\rho}=-\frac{1}{\hbar}\int d^2\vec{r}\Bigg[\frac{\delta}{\delta\rho}\frac{\hbar^2}{2m}\left(\frac{1}{4\rho}(\nabla\rho)^2+(\nabla\theta)^2\delta^2(\vec{r}-\vec{x})\right)\\&\qquad+V\delta^2(\vec{r}-\vec{x})+U\rho\delta^2(\vec{r}-\vec{x})\Bigg]\\&=-\frac{1}{\hbar}\int d^2\vec{r}\left[\frac{\hbar^2}{2m}\left(\frac{1}{2\rho}\nabla\rho\nabla\delta^2(\vec{r}-\vec{x})+\frac{(\nabla\rho)^2}{4\rho^2}\delta^2(\vec{r}-\vec{x})\right)\right]-\frac{\hbar^2}{2m}(\nabla\theta)^2-V-U\rho\\&=-\frac{\hbar^2}{2m}(\nabla\theta)^2-V-U\rho+\frac{\hbar^2}{2m}\left(\frac{\Delta\rho}{2\rho}-\frac{(\nabla\rho)^2}{4\rho^2}\right)\end{aligned}\tag{2.8}$$

where the following expression based on the rearrangement of term $\nabla\rho\nabla\delta^2(\vec{r}-\vec{x})=\nabla\big(\nabla\rho\delta^2(\vec{r}-\vec{x})\big)-(\nabla^2\rho)\delta^2(\vec{r}-\vec{x})$ has been employed, together with the fact that first term vanishes when integrated over a surface S_∞ as a consequence of Green-Gauss theorem.

Finally, the hydrodynamic form of the Gross-Pitaevskii equation is embodied by the set:

$$\begin{cases}\dot{\rho}+\frac{\hbar}{m}\nabla\cdot(\rho\nabla\theta)=0\\ \dot{\theta}+\frac{\hbar^2}{2m}(\nabla\theta)^2=-U\rho-V+\frac{\hbar^2}{2m}\left(\frac{\Delta\rho}{2\rho}-\frac{(\nabla\rho)^2}{4\rho^2}\right)\end{cases}\tag{2.9}$$

where the former one strongly resembles the well-known continuity equation of classical fluid dynamics while the latter is a Bernoulli-like equation, depending on the interaction potential U and an external potential V.

Velocity field and density current field, respectively, are given by:

$$\vec{v}=\frac{\hbar}{m}\nabla\theta=\frac{\hbar}{2mi|\psi|^2}\big(\psi^*\nabla\psi-\psi\nabla\psi^*\big)\tag{2.10}$$

$$\vec{J}=m|\psi|^2\vec{v}\tag{2.11}$$

2.2.1 Thomas-Fermi Approximation

While in the not-interacting regime (e.g. $g=0$) the GPE clearly reduces to the usual Schrödinger equation for which the ground state is well-known. In the

regime of strong repulsive interactions instead we expect a significant difference with respect to the Gaussian wavefunction characterising the previous case. An analytical approach is addressed within the *Thomas-Fermi approximation* [8], which consists in neglecting $\hbar^2$-terms: being the ground state stationary by definition, one finds that $\dot{\rho} = 0 \Rightarrow \nabla\theta = 0$ implying then $\theta = -\mu t$. Together with the second dynamical equation stating that $\dot{\theta} = -\mu = -U\rho - V(\vec{r})$ and that the density profile of the condensate is given by:

$$\rho(\vec{r}) = \frac{\mu}{U}\left(1 - \frac{m\omega^2}{2\mu}r^2\right) = \frac{\mu}{U}\left(1 - \frac{r^2}{R_{TF}^2}\right) \tag{2.12}$$

under the hypotesis of an *harmonic trapping potential* of the form $v(\vec{r}) = m\omega^2 r^2/2$. Being R_{TF} the Thomas-Fermi radius, it is then clear how $\rho \approx const$ could be a reasonable approximation aside from the region $r \to R_{TF}$, as depicted in figure 2.1.

Indeed the agreement between the numerical solution of the GPE and TF profile,

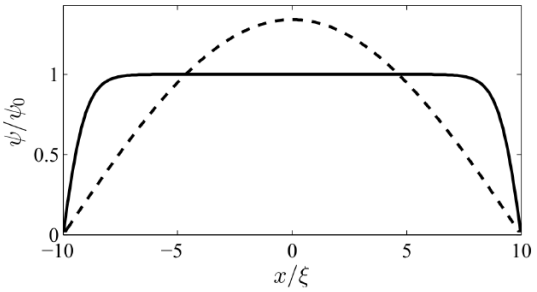

Figure 2.1: Condensate wavefunction as a function of position in the repulsive interaction regime (continuous line) and in the not-interacting regime (dashed line). The profile flattens in almost the entire region, aside from a small region towards the boundary where it rapidly goes to zero.

depicting an inverted parabola as a function of r, is remarkable: Such regime, where kinetic terms (originally $\propto \nabla^2\psi$) can be neglected, falls in the regions where $\rho \to 0$ since the hydrodynamic Hamiltonian presents some divergent terms ($\Delta\rho/\rho$ and $\Delta ln\rho$) that are not accounted within the TF approximation. This is the reason why while in the numerical solution the profile goes to zero asymptotically for $r \to R_{TF}$, TF prediction prescribes a linear behaviour. The critical regions where the Thomas-Fermi approximation loses its validity correspond to the profile's singularities, located in the cores of the vortices.

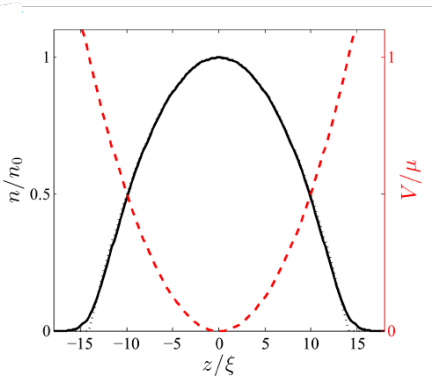

Figure 2.2: Dashed red line represents TF density profile, while the continuous black line depicts the numerical solution of the GPE

2.2.2 Vortex Configurations

In order to exploit the vortex configuration, the case of multiple vortex solution will be analyzed within the TF regime. Field θ has the form

$$\theta(\vec{r},t) = -\mu t + \varphi(\vec{r}) = -\mu t + \text{arctg(y/x)}$$

Plugging such expression in the definition of the velocity field 2.12 then allows to notice that

$$\text{div}\tilde{\text{v}} = \frac{\text{k}}{2\pi}\Delta\theta = 0 \tag{2.13}$$

Moreover from the continuity equation in 2.9 one has $\nabla(\rho\nabla\theta) = \nabla\rho\cdot\nabla\theta + \rho\Delta\theta = 0$ meaning that $\nabla\rho\cdot\nabla\theta = 0$. Assuming a parabolic density profile of the form $\rho \simeq cr^2$ for $\vec{r} \simeq 0$ and $\rho \simeq const$ elsewhere allows to perfectly compensate diverging behaviours (induced by $\Delta\rho/\rho$ and $\Delta ln\rho$) with the profile's singularities for $\vec{r} \to 0$.

Velocity field exhibits a double representation [18], an *electric* and a *magnetic* one respectively:

$$\vec{v} = \frac{k}{2\pi}\nabla\theta = \frac{k}{2\pi}\hat{e}_3 \wedge \frac{\vec{r}}{|\vec{r}|^2} \tag{2.14}$$

$$\vec{v} = \frac{k}{2\pi}\hat{e}_3 \wedge \nabla A = -\frac{k}{2\pi}\text{curl}\big(\text{A}\hat{\text{e}}_3\big) \tag{2.15}$$

thus incorporating two important features in the same mathematical entity:

$$\text{div}(\tilde{\text{v}}) = 0, \quad \text{curl}(\tilde{\text{v}}) = \tilde{\text{w}} \neq 0$$

showing that the fluid is *incompressible* but *rotational*. The scalar field $A = A(\vec{r})$ is defined as:

$$A(\vec{r}) \doteq \frac{1}{2} ln\left(\frac{x^2+y^2}{\lambda^2}\right) \tag{2.16}$$

with parameter λ being the *healing length*, has the structure of a Green Function since $\Delta A(\vec{r}) = 2\pi\delta^2(\vec{r})$. Nevertheless the presence of singularities, embodied by the cores of the vortices, makes field θ singular (for $\vec{r} \to 0$) meaning that the quantity $\nabla\theta = -\text{curl}\big(A\hat{e}_3\big)$ is defined (almost) everywhere except for singular points. This is taken into account by the following argument based on the introduction of *topological classes of curves*.

Consider two closed curves Γ and γ and a singularity located in the origin. As sketched in figure 2.3 the two present a fundamental difference being that one encircles the singular point contained in the origin. This fact acquires more relevance

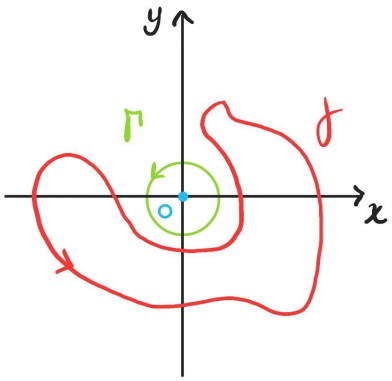

Figure 2.3: Curves Γ (in green) and γ (in red) belong to different topological classes as the former encircles the singularity in the origin, while the latter doesn't contain it.

when evaluating the circulation of the velocity field $\vec{v}$ along the different paths. Indeed along curves of type γ one finds:

$$C = \oint_\gamma d\vec{r}\cdot\vec{v} = \oint_\gamma d\vec{r}\frac{k}{2\pi}\nabla\theta = \frac{k}{2\pi}\int_{\vec{r_1}}^{\vec{r_2}} d\vec{r}\cdot\nabla\theta = \frac{k}{2\pi}\big(\theta(\vec{r_2}) - \theta(\vec{r_1})\big) = 0 \quad (2.17)$$

being $\vec{r_1} = \vec{r_2}$ thus representing the initial and final point of a closed curve. Conversely for Γ-type curves, a different result is obtained:

$$C = \oint_\Gamma d\vec{r}\cdot\vec{v} = \oint_\Gamma d\vec{r}\frac{k}{2\pi}\nabla\theta = \frac{k}{2\pi}\int_0^{2\pi} d\varphi r\hat{e_\varphi}\cdot\left(\hat{e}_3\wedge\frac{\vec{r}}{|\vec{r}|^2}\right) = \frac{k}{2\pi}\int_0^{2\pi} d\varphi = k \quad (2.18)$$

This fundamental difference addresses the distinction between two main classes of curves labelled by a specific *homotopy index* n (referring to the number of times the Γ-type curve wraps around the singularity). This allows to reveal the presence of a vortex that now acquires a *topological character* [8], [18]. In a compact formulation,

given γ a generic curve in the $2D$-space and S_γ the surface with border γ:

$$C = \oint_\gamma d\vec{r}\cdot\vec{v} = \int\int_{S_\gamma} d^2\vec{r}\hat{e}_3\cdot\mathrm{curl}\tilde{\mathrm{v}} = -\frac{\mathrm{k}}{2\pi}\int\int_{\mathrm{S}_\gamma}\mathrm{d}^2\tilde{\mathrm{r}}\hat{\mathrm{e}}_3\mathrm{curl}^2\big(\mathrm{A}\hat{\mathrm{e}}_3\big) = \frac{\mathrm{k}}{2\pi}\int\int_{\mathrm{S}_\gamma}\mathrm{d}^2\tilde{\mathrm{r}}\Delta\mathrm{A} \tag{2.19}$$

in virtue of Stokes' theorem and using the vectorial identity $\nabla\mathrm{div}\tilde{\mathrm{B}} = \Delta\tilde{\mathrm{B}}\mathrm{curl}^2\tilde{\mathrm{B}}$. In the present case where $\vec{B} = A\hat{e}_3$, one can see how $\nabla\mathrm{div}\big(\mathrm{A}\hat{\mathrm{e}}_3\big) = 0$ thus proving the final equivalence in previous equation. Now taking advantage of A being a Green Function, it is possible to verify the existence of a vortex configuration as follows:

$$C = \oint_\gamma d\vec{r}\cdot\vec{v} = \begin{cases} 0 & \text{if } \vec{r} = 0 \notin S_\gamma \\ k & \text{if } \vec{r} = 0 \in S_\gamma \end{cases} \tag{2.20}$$

The relation between circulation C and vortex charge k is prescribed by the so called **Feynman-Onsager condition**

$$\oint_\gamma d\vec{r}\cdot\vec{v} = k \Rightarrow \oint_\gamma d\vec{r}\cdot\vec{p} = mk = 2\pi N\hbar \tag{2.21}$$

and incorporates the *quantization* of the vortex charge (resulting from the Bohr-Sommerfeld quantization process), resulting in

$$k = 2\pi N\frac{\hbar}{m} = N\frac{h}{m} \tag{2.22}$$

In conclusion, a strong analogy between quantum fluids and Bose-Einstein condensates can be outlined by considering the z-component of angular momentum operator:

$$\hat{L}_z = m(\vec{r}\wedge\vec{v})\cdot\hat{e}_3 = \frac{k}{2\pi}m\left[\vec{r}\wedge\left(\hat{e}_3\wedge\frac{\vec{r}}{|\vec{r}|^2}\right)\right]\cdot\hat{e}_3 = \frac{k}{2\pi}m = N\hbar \tag{2.23}$$

such formula shows indeed how all the particles in the superfluid medium possess the same angular momentum (along z-axis). Vortex formation can then be seen as a *condensation phenomena* where quantum state L_z gets macroscopically occupied.

Chapter 3

Point-like Model

"The essence of mathematics is in its freedom."

Georg Cantor

It is known that the description of ultracold bosons passes by the *Gross-Pitaevskii* equations in the so-called *Mean-Field Limit*, non-linear partial differential equations for the (classical) field ψ possessing a space and time dependence. Since such equations can be faced only numerically, a powerful model of recent development in scientific literature is known as the **Point-like Model** [22], [2], [3]that fundamentally allows the reduction of the original mathematical model based on a partial differential equation to a system of coupled ordinary differential equations. Despite the intrinsic non-linearity of the system, the analytical advantage of approaching ODEs contrary to PDEs is evident. This procedure is addressed in first place considering *massless vortices* i.e. vortices whose core, represented by the region where the density profile of the condensate faces a singularity, is assumed empty (see section 2.2) for which a simplified Hamiltonian can be obtained in virtue of some hypotesis. Motion equations naturally follows by means of canonical Poisson Brackets as the system possesses an Hamiltonian structure.

In second place a further level of complexity is introduced by accounting for the presence of core masses leading to the *Massive Point-like Model*: a second-order system resulting from the introduction of 4 new degrees of freedom (v_{x_1}, v_{x_2}, v_{y_1}, v_{y_2}) that is able to account for much more complex and rich dynamics. The presence of massive cores is addressed by means of the *Time Dependent Variational Lagrangian Method* [20], to which a brief section is properly devoted. In chapter 4, dedicated to the algebraic description of the system, it will be properly discussed

how while complete integrability is reached in the massless case due to the presence of a sufficient number of conserved quantities, the introduction of core masses makes the system not-integrable since the number of d.o.f. overtakes the number of prime integrals.

Such analytical model already proved its accuracy through various comparisons with numerical results of the well-known Gross-Pitaevskii equations. Recent works showed how, concerning the case of a pair of massless vortices trapped in a circular box, its dynamics is described by a simple precession motion around the trapping center, while the introduction of increasingly bigger core masses leads to the emergence of instabilities. Moreover the absence of tangential entrainment between the fluids composing the cores and the body of vortices has been established, emphasizing how no dissipation should arise in such rotational dynamics. Highly irregular patterns have also been noticed when asymmetrical initial conditions are introduced.

This chapter is then devoted to the complete derivation of the Point-like model in its massless version at first and then including massive cores together with the resulting dynamical equations.

3.1 The case of free massless vortices

In the general scenario a quantum fluid can present many vortices, requiring a further generalization of the single vortex configuration discussed in section 2.4. Recalling the double representation of the velocity field, in the case of N vortices, the electric picture gives:

$$\begin{aligned}\vec{v}(\vec{r}) &= \sum_i \frac{k_i}{2\pi}\hat{e}_3 \wedge \frac{\vec{r}-\vec{r_i}}{|\vec{r}-\vec{r_i}|^2} = \sum_i \frac{k_i}{2\pi}\nabla\theta_i = \sum_i \frac{N_i}{2\pi}\frac{h}{m}\nabla\theta_i \\ &= \frac{\hbar}{m}\sum_i N_i\nabla\theta_i = \sigma\nabla\theta\end{aligned} \tag{3.1}$$

while the magnetic formulation provides:

$$\begin{aligned}\vec{v}(\vec{r}) &= \sum_i \frac{k_i}{2\pi}\hat{e}_3 \wedge \frac{\vec{r}-\vec{r_i}}{|\vec{r}-\vec{r_i}|^2} = \sum_i \frac{k_i}{2\pi}\hat{e}_3 \wedge \nabla A_i = \sigma\sum_i \hat{e}_3 \wedge N_i\nabla A_i \\ &= \sigma\hat{e}_3 \wedge \nabla A = -\sigma\mathrm{curl}\big(\mathrm{A}\hat{\mathrm{e}}_3\big)\end{aligned} \tag{3.2}$$

where the parameter $\sigma \doteq \hbar/m$ has been introduced, aside from the use of quantization formula 2.22. Fields θ and A are now accounting for multiple contributions

coming from the many vortices in the gas, meaning that

$$\theta(\vec{r}) = \sum_i N_i \theta_i(\vec{r}), \quad A(\vec{r}) = \sum_i N_i A_i(\vec{r}) \tag{3.3}$$

where relations $\nabla\theta_i = \hat{e}_3 \wedge \nabla A_i$ together with $\Delta A = 2\pi \sum_i N_i \delta^2(\vec{r} - \vec{r_i})$ still hold with minimal adjustments.

Presented arguments lead to evaluate the circulation of the velocity field, in the case of a many-vortex configuration, as:

$$\begin{aligned} \oint_\gamma d^2\vec{r} \cdot \vec{v} &= \int\int_{S_\gamma} d\hat{s}\hat{e}_3 \cdot \mathrm{curl}\tilde{\mathrm{v}} = \int\int_{\mathrm{S}_\gamma} \mathrm{d}\hat{\mathrm{s}}\hat{\mathrm{e}}_3 \cdot \hat{\mathrm{e}}_3 \sigma 2\pi \sum_{\mathrm{i}} \mathrm{N_i}\delta^2(\tilde{\mathrm{r}} - \tilde{\mathrm{r}}_{\mathrm{i}}) \\ &= \int\int_{S_\gamma} d\hat{s} \cdot \vec{w} = \sum_i k_i \end{aligned} \tag{3.4}$$

again, in virtue of Stokes' theorem. Motion equations are of trivial derivation as it would be sufficient to evaluate:

$$\dot{\vec{r_j}} = \vec{v}(\vec{r_j}) = \sum_{i \neq j} \frac{k_i}{2\pi} \frac{\hat{e}_3 \wedge \left(\vec{r_j} - \vec{r_i}\right)}{|\vec{r_j} - \vec{r_i}|^2} \tag{3.5}$$

The index $i = j$ has been removed in order to avoid the divergence emerging when two vortices are too close ($\vec{r_i} \to \vec{r_j}$). The same dynamics describing a gas of N free vortices can be exploited passing through a careful manipulation of the hydrodynamic mean-field Hamiltonian.

Indeed one may recall the Hamiltonian arising from the hydrodynamic picture:

$$\mathcal{H} = \int d^2\vec{r} \left[\frac{\hbar^2}{2m} \left(\frac{1}{4\rho} (\nabla\rho)^2 + \rho(\nabla\theta)^2 \right) + V(\vec{r})\rho + \frac{U}{2}\rho^2 \right] \tag{3.6}$$

as properly discussed in section 2.3, the condensate's density profile ρ can be assumed almost constant on the entire domain, aside from the small regions corresponding to the cores of the vortices where it drastically goes to zero in correspondence of the *singularity*. Within the *Point-like Model* an apparently rough approximation is conducted, consisting in the assumption that the density is constant everywhere in the planar domain: $\rho \simeq \rho_0$. Moreover a circular box geometry of radius R is assumed, meaning that confining potential $V(\vec{r})$ has the form:

$$V(\vec{r}) = \begin{cases} 0 & \text{if } \vec{r} < R \\ +\infty & \text{if } \vec{r} = R \end{cases} \tag{3.7}$$

Under this assumptions, the system's Hamiltonian gets approximated as

$$\mathcal{H} \simeq \rho_0 \int_D d^2\vec{r}\left(\frac{\hbar^2}{2m}(\nabla\theta)^2 + V(\vec{r}) + \frac{U_0}{2}\rho_0\right) \simeq \rho_0^2\frac{\hbar^2}{2m}\int_D d^2\vec{r}(\nabla\theta)^2 + \mathcal{C} \tag{3.8}$$

being $\mathcal{C} = U_0\rho_0^2\pi L^2/2$ a constant contribution with L the size of the planar domain. Recalling that $(\nabla\theta)^2 = (\nabla A)^2$ and making use of the well-known vectorial identity

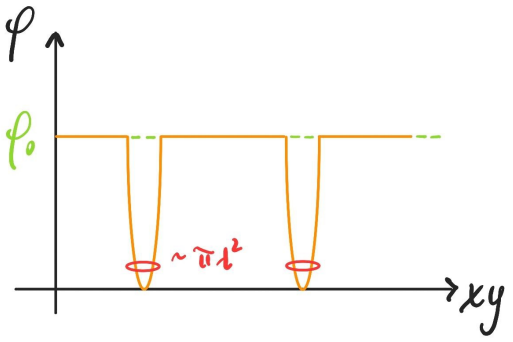

Figure 3.1: Behaviour of the condensate profile with respect to spatial coordinates. The assumption that $\rho(\vec{r}) \simeq \rho_0$ is reasonable almost everywhere, except for the singularities in correspondence of an area of $\approx \pi\lambda^2$.

$(\nabla A)^2 = \mathrm{div}(\mathrm{A}\nabla\mathrm{A}) - \mathrm{A}\Delta\mathrm{A}$, one obtains:

$$\begin{aligned}
\mathcal{H} &\simeq \frac{\rho_0\hbar^2}{2m}\int_D d^2\vec{r}(\nabla A)^2 = \frac{\rho_0\hbar^2}{2m}\int_D d^2\vec{r}\Big(\mathrm{div}(\mathrm{A}\nabla\mathrm{A}) - \mathrm{A}\Delta\mathrm{A}\Big) \\
&= \frac{\rho_0\hbar^2}{2m}\left[\int_D d^2\vec{r}\Big[\hat{e}_3\cdot\mathrm{curl}(\hat{\mathrm{e}}_3\wedge\mathrm{A}\nabla\mathrm{A})\Big]\right. \\
&\left. - \int_D d^2\vec{r}\Big(\sum_i \frac{N_i}{2} ln\frac{|\vec{r}-\vec{r_i}|^2}{\lambda^2}\sum_j 2\pi N_j\delta^2(\vec{r}-\vec{r_j})\Big)\right] \\
&= \frac{\rho_0\hbar^2}{2m}\left[\oint_\Gamma d\vec{r}\cdot(\hat{e}_3\wedge A\nabla A) - \sum_i \frac{N_i}{2} ln\frac{|\vec{r_j}-\vec{r_i}|^2}{\lambda^2}\sum_j 2\pi N_j\right]
\end{aligned} \tag{3.9}$$

where the last equality holds by virtue of Stokes' theorem. Focusing on the first contribution, it is possible to rearrange it as follows, observing that $\nabla A \sim (\vec{r} -$

$\vec{r_i})/|\vec{r}-\vec{r_i}|^2$:

$$\begin{aligned}\mathcal{C}_\infty &= \frac{\rho_0\hbar^2}{2m}\oint_\Gamma d\vec{r}\cdot(\hat{e}_3\wedge A\nabla A) = \frac{\rho_0\hbar^2}{2m}\int_0^{2\pi} Rd\varphi\hat{e_\varphi}\cdot(\hat{e}_3\wedge A\nabla A)\\ &= \frac{\rho_0\hbar^2}{2m}\int_0^{2\pi} Rd\varphi\hat{e_r}\cdot\left(\sum_j\frac{N_j}{2}ln\frac{|\vec{r}-\vec{r_j}|^2}{\lambda^2}\sum_i N_i\frac{\vec{r}-\vec{r_i}}{|\vec{r}-\vec{r_i}|^2}\right)\\ &= \frac{\rho_0\hbar^2}{2m}\int_0^{2\pi} d\varphi\left(\sum_j\frac{N_j}{2}ln\frac{|\vec{r}-\vec{r_j}|^2}{\lambda^2}\sum_i N_i R\hat{e_r}\cdot\frac{\vec{r}-\vec{r_i}}{|\vec{r}-\vec{r_i}|^2}\right)\\ &\overset{R\gg\lambda}{\to}\frac{\rho_0\hbar^2}{2m}\int_0^{2\pi} d\varphi\left(\sum_i N_i\right)^2 ln\left(\frac{R}{\lambda}\right) = \frac{\rho_0\hbar^2}{2m}2\pi\left(\sum_i N_i\right)^2 ln\left(\frac{R}{\lambda}\right)\end{aligned} \tag{3.10}$$

since $\hat{e_r} = \hat{e_\varphi}\wedge\hat{e}_3$. By sending the boundary to infinity, physically obtained in the limit $R\gg\lambda$ meaning that a fictious boundary at high distance ($R\gg|\vec{r_i}|$) is set, then its effects can be neglected and so the term $\vec{r}\cdot(\vec{r}-\vec{r_i})/|\vec{r}-\vec{r_i}|^2\approx 1$ resulting in the last equivalence in previous equation. Such term represents a divergence that does not play any crucial role in the system's dynamics.

In conclusion, it has been proved that Hamiltonian (3.8) can be reduced to the following (see [23]), apart from an infinite constant represented by the term $\mathcal{C}_\infty$:

$$\mathcal{H} = \mathcal{C}_\infty - \frac{\rho_0\hbar^2}{2m}\sum_i N_i ln\frac{|\vec{r_j}-\vec{r_i}|}{\lambda}\sum_j 2\pi N_j = \mathcal{C}_\infty - \frac{\rho_*}{4\pi}\sum_i\sum_{j\neq i}k_i k_j ln\frac{|\vec{r_j}-\vec{r_i}|}{\lambda} \tag{3.11}$$

where has been introduced the parameter $\rho_* \doteq \rho_0 m$ and recalled the expression for the vortex charge $k_i = 2\pi N_i\hbar/m = N_i h/m$. Note that the term $i=j$ has been removed from the summation to neglect an unphysical contribution to the Hamiltonian. This is indeed equivalent to eliminate an area $\approx\lambda^2$ relative to the vortex cores: for $\vec{r}\to\vec{r_j}$ infact, the term $(\nabla\theta)^2\approx 1/|\vec{r}-\vec{r_j}|^2$ features a divergence that must be removed.

However the assumption of $\rho\approx const$ is physically inaccurate, since a real superfluid medium possesses a not uniform density profile that goes to zero close to the vortex cores, compensating the divergent behaviour of $(\nabla\theta)^2$. Nevertheless in the next section it will be proved that despite the choice of a physically reasonable density profile, the expression of the vortex Hamiltonian won't be altered.

Dynamical equations are easily derived through the canonical Poisson Brackets

with respect to canonical variables x_j, y_j such that $\{x_i, y_j\} = \delta_{ij}/(\rho_* k_i)$:

$$\begin{aligned} \dot{x_n} = \{x_n, \mathcal{H}\} &= \frac{1}{\rho_* k_n}\frac{\partial \mathcal{H}}{\partial y_n} = \frac{1}{\rho_* k_n}\frac{\partial}{\partial y_n}\Big(-\frac{\rho_*}{4\pi}\sum_i \sum_{j\neq i} k_i k_j ln\frac{|\vec{r_i} - \vec{r_j}|}{\lambda}\Big) \\ &= -\frac{1}{2\pi k_n}\sum_{i\neq n} k_i k_n \frac{y_n - y_i}{|\vec{r_n} - \vec{r_i}|^2} \end{aligned} \tag{3.12}$$

Similar calculations performed for $\dot{y_n}$ result in the **Helmoltz-Kirchoff equations**

$$\dot{x_n} = -\frac{1}{2\pi}\sum_{i\neq n} k_i \frac{y_n - y_i}{|\vec{r_n} - \vec{r_i}|^2} \tag{3.13}$$

$$\dot{y_n} = \frac{1}{2\pi}\sum_{i\neq n} k_i \frac{x_n - x_i}{|\vec{r_n} - \vec{r_i}|^2} \tag{3.14}$$

perfectly reproducing eq.3.5.

3.1.1 Parabolic density profile in the proximity of cores

Previously a rough approximation on the condensate's density profile has been considered, assuming it flat in all of the occupied space. With the goal of performing a more "gentle" approximation, it is possible to assume the existence of a series of subdomains D_k, each one covering an approximate area $D_0 \simeq \pi\lambda^2$, where the condensate has a non-trivial density profile $\rho(r) = c|\vec{r} - \vec{r_k}|^2$, while it remains constant $\rho \simeq \rho_0$ in every other point of the domain D_0. Formally speaking, the density profile is assumed to be:

$$\rho = \begin{cases} \rho_0 & \text{if } \vec{r} \in D_0 \\ c|\vec{r} - \vec{r_k}|^2 & \text{if } \vec{r} \in D_k \end{cases} \tag{3.15}$$

This way the overall planar domain can be expressed as a partition of sub-regions:

$$D = D_0 \cup_k D_k$$

Through this assumption it is possible to adapt Hamiltonian (3.8) in the following way:

$$\begin{aligned} \mathcal{H} &= \frac{\hbar^2}{2m}\int_{D_0} d^2\vec{r}\Big[\frac{\rho}{4}(\nabla ln\rho)^2 + \rho(\nabla\theta)^2\Big] + \sum_k \left[\frac{\hbar^2}{2m}\int_{D_k} d^2\vec{r}\Big[\frac{\rho}{4}(\nabla ln\rho)^2 + \rho(\nabla\theta)^2\Big]\right] \\ &\simeq \frac{\hbar^2}{2m}\left[\rho_0\int_{D_0} d^2\vec{r}(\nabla\theta)^2 + \sum_k \int_{D_k} d^2\vec{r}\Big[c + c|\vec{r} - \vec{r_k}|^2(\nabla\theta)^2\Big]\right] \end{aligned} \tag{3.16}$$

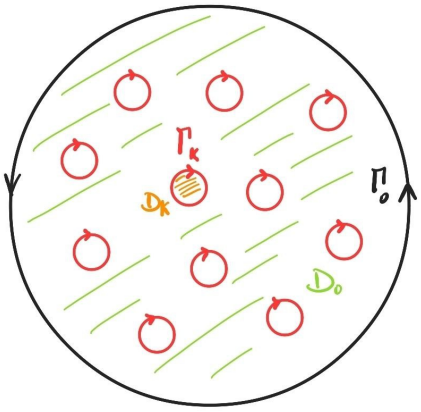

Figure 3.2: Partition of planar domain D as the union of k subdomains and the region D_0. Note that curves Γ_k and Γ_0 are clockwise and counterclockwise respectively to ensure the evalutation of the overall line integral over D.

where has been exploited the fact that:

$$\frac{\rho}{4}(\nabla ln\rho)^2 = \frac{c}{4}|\vec{r}-\vec{r_k}|^2\left(\frac{\nabla\rho}{\rho}\right)^2 = \frac{c}{4}|\vec{r}-\vec{r_k}|^2\left(\frac{2c|\vec{r}-\vec{r_k}|}{c|\vec{r}-\vec{r_k}|^2}\right)^2 = c$$

Now considering the fact that the fiels θ can be expressed as a superposition of many local θ_i-fields, the integration over disk D_k leads to the simplification:

$$\nabla\theta = \sum_i N_i\hat{e}_3\wedge\frac{\vec{r}-\vec{r_i}}{|\vec{r}-\vec{r_i}|^2} = N_k\hat{e}_3\wedge\frac{\vec{r}-\vec{r_k}}{|\vec{r}-\vec{r_k}|^2}+\sum_{i\neq k} N_i\hat{e}_3\wedge\frac{\vec{r}-\vec{r_i}}{|\vec{r}-\vec{r_i}|^2} \simeq N_k\hat{e}_3\wedge\frac{\vec{r}-\vec{r_k}}{|\vec{r}-\vec{r_k}|^2}$$

since the subdomains D_k are far enough and thus the influence of all components θ_i with $i \neq k$ becomes negligible. This allows to approximate the Hamiltonian to:

$$\begin{aligned}
\mathcal{H} &= \frac{m\sigma^2}{2}\left[\sum_k 2c\pi\lambda^2 + \sum_k\int_{D_k} d^2\vec{r}\left[c|\vec{r}-\vec{r_k}|^2\left(\sum_i N_i\hat{e}_3\wedge\frac{\vec{r}-\vec{r_i}}{|\vec{r}-\vec{r_i}|^2}\right)\right]\right. \\
&\qquad\left. + \rho_0\int_{D_0} d^2\vec{r}(\nabla\theta)^2\right] \\
&\simeq \frac{m\sigma^2}{2}\left[\sum_k 2c\pi\lambda^2 + \sum_k\int_{D_k} d^2\vec{r}c|\vec{r}-\vec{r_k}|^2N_k^2\frac{|\vec{r}-\vec{r_k}|^2}{|\vec{r}-\vec{r_k}|^4} + \rho_0\int_{D_0} d^2\vec{r}(\nabla\theta)^2\right] \\
&= \frac{m\sigma^2}{2}\left[\sum_k\left(2c\pi\lambda^2+\pi\lambda^2cN_k^2\right) + \rho_0\int_{D_0} d^2\vec{r}(\nabla\theta)^2\right]
\end{aligned} \tag{3.17}$$

In the case of a free boson mixture (e.g. for $R \gg \lambda$) it is possible to further rearrange the previous expression noticing the emergence of a constant contribution

$$\mathcal{C}(\lambda) = \frac{m\sigma^2}{2}\left[\sum_k \left(2c\pi\lambda^2 + \pi\lambda^2 c N_k^2\right)\right] \tag{3.18}$$

that doesn't play any role in the derivation of dynamical equation. Indeed

$$\begin{aligned}\mathcal{H} &= \mathcal{C}(\lambda) + \frac{m\sigma^2}{2}\int_{D_0} d^2\vec{r}\rho_0(\nabla\theta)^2 = \mathcal{C}(\lambda) + \frac{m\rho_0\sigma^2}{2}\int_{D_0}\Big[\mathrm{div}(\mathrm{A}\nabla\mathrm{A}) - \mathrm{A}\Delta\mathrm{A}\Big] \\ &= \mathcal{C}(\lambda) + \frac{m\sigma^2}{2}\Big[\oint_\Gamma d\vec{r}\cdot(\hat{e}_3 \wedge A\nabla A) - \int_{D_0}\sum_i \frac{N_i}{2} ln\frac{|\vec{r}-\vec{r_i}|^2}{\lambda^2}\sum_j 2\pi N_j\delta^2(\vec{r}-\vec{r_j})\Big]\end{aligned} \tag{3.19}$$

where the last term vanishes in virtue of the definition of the delta function: in the domain D_0 infact, $\delta^2(\vec{r}-\vec{r_j}) = 0$. Thus considering the remaining term, the line integral can be rearranged observing that it represents the circulation along the overall domain D_0, whose border can be written as $\Gamma = \Gamma_0 \cup (\sum_k \Gamma_k)$ as depicted in figure 3.1. The curves Γ_k infact reflect circulations over the boundary of the $k-th$ subdomain where density singularities are present. This way one obtains:

$$\begin{aligned}\oint_\Gamma d\vec{r}\cdot(\hat{e}_3 \wedge A\nabla A) &= \oint_{\Gamma_0} d\vec{r}\cdot(\hat{e}_3 \wedge A\nabla A) - \sum_k \oint_{\Gamma_k} d\vec{r}\cdot(\hat{e}_3 \wedge A\nabla A) \\ &\overset{R\gg\lambda}{\to} \mathcal{C}_\infty - \sum_k \oint_{\Gamma_k} d\vec{r}\cdot(\hat{e}_3 \wedge A\nabla A)\end{aligned}$$

where the line integral over Γ_0 represent a diverging contribution in the $R \gg \lambda$ limit, e.g. by sending the boundary to infinity and so considering a free vortex gas. In conclusion, Hamiltonian (3.8) in the case of a parabolic density profile

reduces to:

$$\begin{aligned}
\mathcal{H} &= \mathcal{C}(\lambda) + \mathcal{C}_\infty - \frac{m\rho_0\sigma^2}{2}\sum_k \oint_{\Gamma_k} d\vec{r}\cdot(\hat{e}_3 \wedge A\nabla A) \\
&= \mathcal{C}(\lambda) + \mathcal{C}_\infty - \frac{m\rho_0\sigma^2}{2}\sum_k A(\vec{r_k}) \oint_{\Gamma_k} d\vec{r}\cdot(\hat{e}_3 \wedge \nabla A) \\
&= \mathcal{C}(\lambda) + \mathcal{C}_\infty - \frac{m\rho_0\sigma^2}{2}\sum_k A(\vec{r_k}) \oint_{\Gamma_k} d\vec{r}\cdot\nabla\theta \\
&= \mathcal{C}(\lambda) + \mathcal{C}_\infty - \frac{m\rho_0\sigma^2}{2}\sum_k A(\vec{r_k}) \oint_{\Gamma_k} d\vec{r}\cdot\left(N_k\nabla\theta_k + \sum_{j\neq k} N_j\nabla\theta_j\right) \\
&= \mathcal{C}(\lambda) + \mathcal{C}_\infty - \frac{m\rho_0\sigma^2}{2}\sum_k A(\vec{r_k})(2\pi N_k) \\
&= \mathcal{C}(\lambda) + \mathcal{C}_\infty - \frac{m\rho_0\sigma^2}{2}\sum_k\sum_j \frac{N_j}{2} ln\frac{|\vec{r_k} - \vec{r_j}|^2}{\lambda^2} 2\pi N_k
\end{aligned} \tag{3.20}$$

in virtue of the approximation $\sum_k \oint_{\Gamma_k} d\vec{r}\cdot(\hat{e}_3\wedge A\nabla A) \simeq \sum_k A(\vec{r_k}) \oint_{\Gamma_k} d\vec{r}\cdot(\hat{e}_3\wedge\nabla A)$ justified by the fact that the field A can be shown to be almost constant in the surroundings of the integration domain Γ_k.

Previous calculations then lead to:

$$\mathcal{H} = \mathcal{C}(\lambda) + \mathcal{C}_\infty - \frac{\rho_*}{4\pi}\sum_k\sum_{j\neq k} k_k k_j ln\frac{|\vec{r_k} - \vec{r_j}|}{\lambda} \tag{3.21}$$

showing how, despite the introduction of a more physical approximation for the condensate's density profile, the same Hamiltonian has been found. Since no improvements in the model have been made, in the following discussions the original approximation $\rho \approx const$ will be considered as it proves to capture the same amount of physical informations as the parabolic profile.

3.2 The inclusion of boundary effects

The inclusion of boundaries or obstacles in the domain is addressed by means of the **Virtual Charge Method**, typically employed in Electrostatics and Fluid Dynamics to account for walls or obstacles in the domain. Considering a particle with charge $+e$ in position $\vec{r} = (x, y)$, the presence of a wall in position $x = 0$ is addressed by assuming the existence of a *virtual* particle with charge $-e$ in position $\vec{r}^* = (x^*, y^*) = (-x, y)$. The same principle applies to the vortex gas case,

where each virtual vortex possesses an opposite circulation $-k$.

In the simplest scenario the vortices can be thought as confined in a half-plane $D = \mathbb{R}^+$, while virtual vortices are positioned at $\vec{r_i} = (x_i^*, y_i^*) = (-x_i, y_i)$. This way it becomes necessary to introduce:

$$\theta_{tot} \doteq \theta(\vec{r}) + \bar{\theta}(\vec{r}) = \sum_i N_i \mathrm{arctg}\Big(\frac{\mathrm{y} - \mathrm{y_i}}{\mathrm{x} - \mathrm{x_i}}\Big) - \sum_i N_i \mathrm{arctg}\Big(\frac{\mathrm{y} - \mathrm{y_i^*}}{\mathrm{x} - \mathrm{x_i^*}}\Big) \tag{3.22}$$

and similarly

$$A_{tot} \doteq A(\vec{r}) + \bar{A}(\vec{r}) = \sum_i \frac{N_i}{2} ln \frac{|\vec{r} - \vec{r_i}|^2}{\lambda^2} - \sum_i \frac{N_i}{2} ln \frac{|\vec{r} - \vec{r_i^*}|^2}{\lambda^2} \tag{3.23}$$

Hamiltonian (3.8) then can be treated as follows, taking advantage of the well-known vectorial identity concerning $(\nabla A)^2$:

$$\begin{aligned} \mathcal{H} &\simeq \rho_0 \frac{\hbar^2}{2m} \int_D d^2\vec{r} (\nabla\theta)^2 = \rho_0 \frac{m\sigma^2}{2} \int_D d^2\vec{r} (\nabla A_{tot})^2 \\ &= \rho_0 \frac{m\sigma^2}{2} \int_D d^2\vec{r} \Big[\mathrm{div}(\mathrm{A_{tot}} \nabla \mathrm{A_{tot}}) - \mathrm{A_{tot}} \Delta \mathrm{A_{tot}} \Big] \end{aligned} \tag{3.24}$$

To exploit the second integral, it is possible to rearrange its argument in the following way:

$$\begin{aligned} A_{tot} \Delta A_{tot} &= \left(\sum_i \frac{N_i}{2} ln \frac{|\vec{r} - \vec{r_i}|^2}{\lambda^2} - \sum_i \frac{N_i}{2} ln \frac{|\vec{r} - \vec{r_i^*}|^2}{\lambda^2} \right) \\ &\times \left(\sum_j 2\pi N_j \delta^2(\vec{r} - \vec{r_j}) - \sum_j 2\pi N_j \delta^2(\vec{r} - \vec{r_j^*}) \right) \\ &= \sum_i \frac{N_i}{2} ln \frac{|\vec{r} - \vec{r_i}|^2}{\lambda^2} \sum_j 2\pi N_j \delta^2(\vec{r} - \vec{r_j}) \\ &- \sum_i \frac{N_i}{2} ln \frac{|\vec{r} - \vec{r_i^*}|^2}{\lambda^2} \sum_j 2\pi N_j \delta^2(\vec{r} - \vec{r_j}) \end{aligned} \tag{3.25}$$

where the term $\delta^2(\vec{r} - \vec{r_j^*})$ is trivially null since we are performing the integration over the domain D where virtual vortices are not present. Thus its integral

becomes:

$$\begin{aligned}
\rho_0 \frac{m\sigma^2}{2} \int_D d^2\vec{r} \Bigg[\Bigg(\sum_i \frac{N_i}{2} ln \frac{|\vec{r} - \vec{r_i}|^2}{\lambda^2} \sum_j 2\pi N_j \delta^2(\vec{r} - \vec{r_j}) \\
- \sum_i \frac{N_i}{2} ln \frac{|\vec{r} - \vec{r_i^*}|^2}{\lambda^2} \sum_j 2\pi N_j \delta^2(\vec{r} - \vec{r_j}) \Bigg] \\
= \rho_0 \frac{m\sigma^2}{2} \left(\frac{1}{2} \sum_i \sum_{j \neq i} 2\pi N_i N_j ln \frac{|\vec{r_j} - \vec{r_i}|^2}{\lambda^2} - \frac{1}{2} \sum_i \sum_j 2\pi N_i N_j ln \frac{|\vec{r_j} - \vec{r_i^*}|^2}{\lambda^2} \right) \\
= \frac{\rho_*}{4\pi} \left[\frac{1}{2} \sum_i \sum_{j \neq i} k_i k_j ln \frac{|\vec{r_j} - \vec{r_i}|^2}{\lambda^2} - \frac{1}{2} \sum_i \sum_j k_i k_j ln \frac{|\vec{r_j} - \vec{r_i^*}|^2}{\lambda^2} \right]
\end{aligned} \tag{3.26}$$

where has been introduced $\rho_* \doteq \rho m$ and recalled the expression for the vortex charge $k = 2\pi N\hbar/m = Nh/m$. Note that the summations have been separated in order to eliminate one term corresponding to $i = j$ for which the logarithm function is not defined.

The first contribution in equation (3.24) can be instead manipulated thanks to Stokes' theorem, introducing Γ as a curve that encircles D: such curve can be thought as the union of the y-axis and a semicircumference that lies in the half-plane $\mathbb{R}^+$ as showed in figure 3.3. Though $\Gamma = \gamma \cup \gamma_R$ leads to:

$$\begin{aligned}
\mathcal{C}(\Gamma) &= \rho_0 \frac{m\sigma^2}{2} \int_D d^2\vec{r} \Big[\mathrm{div}(\mathrm{A_{tot}} \nabla \mathrm{A_{tot}}) \Big] \\
&= \rho_0 \frac{m\sigma^2}{2} \int_D d^2\vec{r} \Big[\hat{e}_3 \cdot \mathrm{curl}(\hat{\mathrm{e}}_3 \wedge \mathrm{A_{tot}} \nabla \mathrm{A_{tot}}) \Big] \\
&= \rho_0 \frac{m\sigma^2}{2} \oint_\Gamma d\vec{r} \cdot \Big[\hat{e}_3 \wedge A_{tot} \nabla A_{tot} \Big] \\
&= \rho_0 \frac{m\sigma^2}{2} \left(\oint_\Gamma d\vec{r} \cdot \Big[\hat{e}_3 \wedge A_{tot} \nabla A_{tot} \Big] + \int_{\gamma_R} d\vec{r} \cdot \Big[\hat{e}_3 \wedge A_{tot} \nabla A_{tot} \Big] \right)
\end{aligned} \tag{3.27}$$

recalling the identity $\hat{e_r} = \hat{e_\varphi} \wedge \hat{e}_3$ and being R the radius of γ_R. Observing that both $A_{tot} = const \equiv 0$ along γ (the y-axis) and that $A_{tot}(R) = const \equiv 0$ along semicircumference γ_R, one may conclude that $\mathcal{C}(\Gamma) \equiv 0$. Finally, the systems'

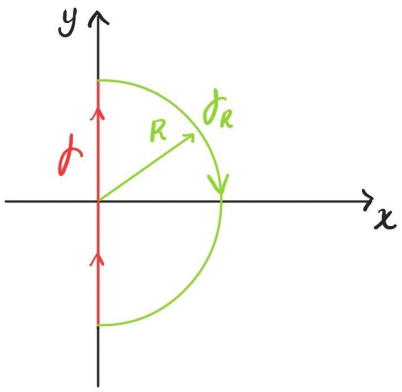

Figure 3.3: Sketch of how the curve laying on the wall can be considered as a closed curve made by the union of the y-axis γ and the semicircumference $\gamma_R \in \mathbb{R}^+$.

Hamiltonian reduces to:

$$\mathcal{H} = -\frac{\rho_*}{4\pi}\left[\sum_i \sum_{j\neq i} k_i k_j ln\frac{|\vec{r_j} - \vec{r_i}|^2}{\lambda^2} - \frac{1}{2}\sum_i \sum_{j\neq i} k_i k_j ln\frac{|\vec{r_j} - \vec{r_i^*}|^2}{\lambda^2} - \frac{1}{2}\sum_i k_i^2 ln\frac{|\vec{r_i} - \vec{r_i}^*|^2}{\lambda^2}\right] \tag{3.28}$$

then by exploiting the expression of the conformal transformation for the positions of the virtual vortices, one obtains:

$$\mathcal{H} = -\frac{\rho_*}{4\pi}\frac{1}{2}\sum_i \sum_{j\neq i} k_i k_j ln\frac{|\vec{r_j} - \vec{r_i}|^2}{|\vec{r_j} - \vec{r_i^*}|^2} + \frac{\rho_*}{4\pi}\frac{1}{2}\sum_i k_i^2 ln\frac{x_i^2}{\lambda^2} \tag{3.29}$$

3.2.1 Circular confinement and disk-like obstruction

To model a confinement effect in a circular box of radius R, one must exploit a suitable *conformal transformation* linking the $i-th$ real vortex position with the position of its corresponding anti-vortex. This is expressed through:

$$\vec{r_i^*} = \vec{r_i}\frac{R^2}{|\vec{r_i}|^2} \tag{3.30}$$

This way it becomes necessary to recall:

$$\theta_{tot} \doteq \theta(\vec{r}) + \bar{\theta}(\vec{r}) = \sum_i N_i \text{arctg}\left(\frac{\text{y} - \text{y}_\text{i}}{\text{x} - \text{x}_\text{i}}\right) - \sum_i N_i \text{arctg}\left(\frac{\text{y} - \text{y}_\text{i}^*}{\text{x} - \text{x}_\text{i}^*}\right) \tag{3.31}$$

while potential A_{tot}

$$\begin{aligned} A_{tot} &\doteq A(\vec{r}) + \bar{A}(\vec{r}) \\ &= \sum_i \frac{N_i}{2} ln \frac{|\vec{r} - \vec{r_i}|^2}{\lambda^2} - \sum_i \frac{N_i}{2} ln \frac{|\vec{r} - \vec{r_i^*}|^2}{\lambda^2} \end{aligned} \tag{3.32}$$

Accounting for these revised potentials and assuming again a flat density profile, it is possible to perform some manipulations on Hamiltonian (3.8), observing that if $\rho \simeq const$ then $(\nabla ln\rho) = 0$:

$$\mathcal{H} \simeq \rho_0 \frac{\hbar^2}{2m} \int_D d^2\vec{r} (\nabla\theta)^2 = \rho_0 \frac{m\sigma^2}{2} \int_D d^2\vec{r} \Big[\mathrm{div}(\mathrm{A_{tot}} \nabla \mathrm{A_{tot}}) - \mathrm{A_{tot}} \Delta \mathrm{A_{tot}} \Big] \tag{3.33}$$

where has been introduced the parameter $\sigma \doteq \hbar/m$. In the second integral the expression concerning potential A_{tot} can be reformulated noticing that $A_{tot}\Delta A_{tot} = (A + \bar{A})\Delta(A + \bar{A})$, leading to:

$$\begin{aligned} &\frac{m\rho_0\sigma^2}{2} \int_D d^2\vec{r} \Big[A_{tot} \Delta A_{tot} \Big] \\ &\quad = \frac{m\rho_0\sigma^2}{2} \int_D d^2\vec{r} \Bigg[\sum_i \frac{N_i}{2} \left(ln \frac{|\vec{r} - \vec{r_i}|^2}{\lambda^2} - ln \frac{|\vec{r} - \vec{r_i}^*|^2}{\lambda^2} \right) \\ &\quad \times \sum_j 2\pi N_j \Big(\delta^2(\vec{r} - \vec{r_j}) - \delta^2(\vec{r} - \vec{r_j}^*) \Big) \Bigg] \\ &\quad = \frac{m\rho_0\sigma^2}{2} \left[\sum_i \frac{N_i}{2} \left(ln \frac{|\vec{r_j} - \vec{r_i}|^2}{\lambda^2} - ln \frac{|\vec{r_j} - \vec{r_i}^*|^2}{\lambda^2} \right) \right] \sum_j 2\pi N_j \\ &\quad = \frac{\rho_*}{4\pi} \left[\sum_i \sum_{i \neq j} k_i k_j ln \frac{|\vec{r_j} - \vec{r_i}|}{\lambda} - \sum_i \sum_j k_i k_j ln \frac{|\vec{r_j} - \vec{r_i}^*|}{\lambda} \right] \end{aligned} \tag{3.34}$$

where the term $\delta^2(\vec{r} - \vec{r_j^*})$ is null since we are performing the integration over the domain D where no virtual vortices are present and again from the first summations it has been removed the term $i = j$ in order to eliminate the emergence of a diverging behaviour. Moreover it have been introduced $\rho_* \doteq \rho m$ and the expression for the vortex charge $k = 2\pi N\hbar/m = Nh/m$.

The first integral in equation (3.33) can be instead manipulated by virtue of

Stokes' theorem. Introducing γ as a curve of radius R that encircles D and recalling the identity $\hat{e_r} = \hat{e_\varphi} \wedge \hat{e}_3$:

$$\begin{aligned}
\mathcal{C}(\gamma) &= \frac{m\rho_0\sigma^2}{2}\int_D d^2\vec{r}\Big[\mathrm{div}(\mathrm{A_{tot}}\nabla\mathrm{A_{tot}})\Big] = \frac{\mathrm{m}\rho_0\sigma^2}{2}\int_\mathrm{D}\mathrm{d}^2\tilde{\mathrm{r}}\Big[\hat{\mathrm{e}}_3\cdot\mathrm{curl}(\hat{\mathrm{e}}_3\wedge\mathrm{A_{tot}}\nabla\mathrm{A_{tot}})\Big] \\
&= \frac{m\rho_0\sigma^2}{2}\oint_\Gamma d\vec{r}\cdot\Big[\hat{e}_3\wedge A_{tot}\nabla A_{tot}\Big] = \frac{m\rho_0\sigma^2}{2}\int_0^{2\pi} Rd\varphi\hat{e_\varphi}\cdot\Big[\hat{e}_3\wedge A_{tot}\nabla A_{tot}\Big] \\
&\simeq \frac{m\rho_0\sigma^2}{2}A_{tot}(\vec{R})\int_0^{2\pi} Rd\varphi\hat{e_\varphi}\cdot\Big[\hat{e}_3\wedge\nabla A_{tot}\Big] \\
&= \frac{m\rho_0\sigma^2}{2}A_{tot}(\vec{R})\int_0^{2\pi} Rd\varphi\hat{e_\varphi}\cdot(\nabla\theta_{tot})
\end{aligned} \tag{3.35}$$

thanks to the relation $\nabla\theta_i = \hat{e}_3\wedge\nabla A_i$. Previous approximation is justified once again by the fact that potential A_{tot} is almost constant in the surroundings of the singularity. Observing now that $\nabla\theta_i = \hat{e}_3\wedge\vec{r_i}/|\vec{r}|^2$, then the final expression of diverging constant $\mathcal{C}(\gamma)$ reads:

$$\begin{aligned}
\mathcal{C}(\gamma) &= \frac{m\rho_0\sigma^2}{2}A_{tot}(\vec{R})\int_0^{2\pi} Rd\varphi\hat{e_\varphi}\cdot\Big(\sum_i N_i\hat{e}_3\wedge\frac{\vec{r_i}}{|\vec{r}|^2}\Big) \\
&= \frac{m\rho_0\sigma^2}{2}A_{tot}(\vec{R})\int_0^{2\pi} d\varphi\sum_i N_i = \frac{m\rho_0\sigma^2}{2}A_{tot}(\vec{R})2\pi\sum_i N_i \\
&= \frac{\rho_*}{4\pi}(\sum_i k_i)\sum_j k_j ln\frac{|\vec{R}-\vec{r_j}|^2}{|\vec{R}-\vec{r_j}^*|^2}
\end{aligned} \tag{3.36}$$

where the relation $\vec{r}\cdot(\vec{r}-\vec{r_i})/|\vec{r}-\vec{r_i}|^2 \approx 1$ has been exploited. Such result shows how the overall term $\int_D A_{tot}\nabla A_{tot}$ from eq. (3.33) can be reduced to a constant that represents a negligible contribution in the system's dynamics. In conclusion we obtain the following Hamiltonian:

$$\begin{aligned}
\mathcal{H} = \mathcal{C}(\gamma) &- \frac{\rho_*}{4\pi}\Bigg[\frac{1}{2}\sum_i\sum_{j\neq i}k_ik_jln\frac{|\vec{r_j}-\vec{r_i}|^2}{\lambda^2} - \frac{1}{2}\sum_i\sum_{j\neq i}k_ik_jln\frac{|\vec{r_j}-\vec{r_i^*}|^2}{\lambda^2} \\
&\qquad - \frac{1}{2}\sum_i k_i^2 ln\frac{|\vec{r_i}-\vec{r_i}^*|^2}{\lambda^2}\Bigg] \\
= -\frac{\rho_*}{4\pi}&\Bigg[\sum_i\sum_{j\neq i}k_ik_jln\Big(\frac{R^2-2\vec{r_i}\cdot\vec{r_j}+|\vec{r_j}|^2|\vec{r_i}|^2/R^2}{|\vec{r_j}|^2-2\vec{r_j}\cdot\vec{r_i}+|\vec{r_i}|^2}\Big) - \sum_i k_i^2 ln\Big(1-\frac{|\vec{r_i}|^2}{R^2}\Big)\Bigg]
\end{aligned} \tag{3.37}$$

where in the last line the proper expression of the conformal transformation $\vec{r_i}^* \doteq \vec{r_i}R^2/|\vec{r_i}|^2$ has been plugged, together with the form of constant $\mathcal{C}(\gamma)$. It is important to notice that by inverting the conformal transformation concerning the position of the $i-th$ antivortex it is possible to invert the physical setting by keeping unchanged the system's Hamiltonian. This way the vortices *outside* the boundary can be considered as real vortices (while previously were considered as virtual ones) and the ones *inside* are now their corresponding virtual images. Infact while in the original formulation the model is meant to describe N vortices confined *inside* the circular boundary, in the present work the purpose is to investigate the behaviour of vortices laying *outside* and colliding against it. This equivalence can be simply proven by revising potentials θ and A by inverting the role of real and virtual vortices. This leads to changing $N_i \to -N_i$ and renominate $\vec{r_i} \to \vec{s_i}^*, \vec{r_i}^* \to \vec{s_i}$ in the expression of potential 3.32:

$$\begin{aligned} A'_{tot} &\doteq A'(\vec{r}) + \bar{A}'(\vec{r}) + A_0(\vec{r}) \\ &= -\sum_i \frac{N_i}{2} ln \frac{|\vec{r}-\vec{r_i}|^2}{\lambda^2} + \sum_i \frac{N_i}{2} ln \frac{|\vec{r}-\vec{r_i}^*|^2}{\lambda^2} + \sum_i N_i A_0(\vec{r}) \\ &= \sum_i \frac{N_i}{2} ln \frac{|\vec{r}-\vec{s_i}|^2}{\lambda^2} - \sum_i \frac{N_i}{2} ln \frac{|\vec{r}-\vec{s_i}^*|^2}{\lambda^2} + \frac{1}{2} ln\left(\frac{|\vec{r}|^2}{\lambda^2}\right) \sum_i N_i \end{aligned} \tag{3.38}$$

It now possesses an extra term A_0 that in the $\vec{R} \to 0$ limit (e.g. when the size of the obstacle is vanishingly small) cancels the terms arising from virtual vortices allowing to reproduce the original vector potential of N free vortices in the plane. Indeed for $\vec{R} \to 0$ virtual vortices collapse in the origin $s_i = |\vec{s_i}| = R^2/s_i^* \to 0$ and such contributions are cancelled out thanks to A_0. Being A_{tot} still a Green function, it now satisfies

$$\Delta A_{tot} = 2\pi \sum_i N_i \big(\delta^2(\vec{r}-\vec{s_i}^*) - \delta^2(\vec{r}-\vec{s_i})\big) + 2\pi\delta^2(\vec{r}) \sum_i N_i \tag{3.39}$$

Moreover, previous additive term A_0 produces an extra contribution in the velocity field $\vec{v}(\vec{r})$ that becomes

$$\vec{v}(\vec{r}) = \sum_i \left[\frac{k_i}{2\pi}\hat{e}_3 \wedge \frac{\vec{r}-\vec{s_i}}{|\vec{r}-\vec{s_i}|^2} - \frac{k_i}{2\pi}\hat{e}_3 \wedge \frac{\vec{r}-\vec{s_i}^*}{|\vec{r}-\vec{s_i}^*|^2}\right] + \frac{1}{2\pi}\left(\sum_i k_i\right)\hat{e}_3 \wedge \frac{\vec{r}}{|\vec{r}|^2} \tag{3.40}$$

Plugging the new potential $A^{'}_{tot}$ in equation (3.33) results in the modification of its second contribution (given by (3.34)) as:

$$\begin{aligned}
&\frac{m\rho_0\sigma^2}{2}\int_D \left[A^{'}_{tot}\Delta A^{'}_{tot}\right] \\
&\quad= \frac{\rho_*}{4\pi}\left[\sum_i\sum_{j\neq i} k_ik_j ln\frac{|\vec{r_j}^* - \vec{r_i}^*|^2}{\lambda^2} - \sum_i\sum_j k_ik_j ln\frac{|\vec{r_j}^* - \vec{r_i}|^2}{\lambda^2} + \sum_i N_iA_0(\vec{r_i})\right] \\
&\quad= \frac{\rho_*}{4\pi}\left[\sum_i\sum_{j\neq i} k_ik_j ln\frac{|\vec{s_j} - \vec{s_i}|^2}{\lambda^2} - \sum_i\sum_j k_ik_j ln\frac{|\vec{s_j} - \vec{s_i}^*|^2}{\lambda^2}\right. \\
&\qquad\qquad\left. + \frac{1}{2}\left(\sum_j N_j\right)\sum_i N_i ln\frac{|\vec{s_i}|^2}{\lambda^2}\right]
\end{aligned} \tag{3.41}$$

since $\delta^2(\vec{r}-\vec{r_j}^*) = \delta^2(\vec{s}-\vec{s_j})$ is now an active contribution. We are still performing the integration over the domain D but as the role of vortex and anti-vortex has been inverted, no (new) virtual vortex $\vec{s_j}^*$ is present. For the same reason, from the first summations it has been removed the term $i = j$ to prevent from an unphysical contribution to $\mathcal{H}$. Conversely the first of term in 3.33 gets modified as follows

$$\begin{aligned}
&\frac{m\rho_0\sigma^2}{2}\int_D d^2\vec{r}\Big[\mathrm{div}(\mathrm{A_{tot}}\nabla\mathrm{A_{tot}})\Big] = \mathcal{C}(\Gamma) - \mathcal{C}(\gamma) \\
&\quad= \frac{m\rho_0\sigma^2}{2}\left[\oint_\Gamma d\vec{r}\cdot\Big[\hat{e}_3\wedge A_{tot}\nabla A_{tot}\Big] - \oint_\gamma d\vec{r}\cdot\Big[\hat{e}_3\wedge A_{tot}\nabla A_{tot}\Big]\right]
\end{aligned} \tag{3.42}$$

considering γ as a curve of radius $\vec{R}$ representing the disk boundary and introducing a second curve Γ, a circle of radius $\vec{r}\to\infty$ encircling the plane with opposite directions. By noticing that

$$\sum_i\left(N_iA_i(\vec{r}) - N_i\bar{A}_i(\vec{r})\right) = \sum_i\frac{N_i}{2}ln\frac{|\vec{r}-\vec{s_i}|^2}{|\vec{r}-\vec{s_i}^*|^2}\to 0, \quad \vec{r}\to+\infty$$

and that $A_0(\vec{r})$ is constant along curve Γ, one may write

$$\begin{aligned}
\mathcal{C}(\Gamma) &= \frac{m\rho_0\sigma^2}{2}\oint_\Gamma d\vec{r}\cdot\Big[\hat{e}_3\wedge A_{tot}\nabla A_{tot}\Big] = \frac{m\rho_0\sigma^2}{2}A_0(\vec{r})\sum_i N_i \\
&= \frac{m\rho_0\sigma^2}{2}2\pi\left(\sum_i N_i\right)^2\frac{1}{2}ln\left(\frac{|\vec{r}|^2}{\lambda^2}\right)\to+\infty, \quad \text{for} \quad \vec{r}\to+\infty
\end{aligned} \tag{3.43}$$

thus representing a diverging constant. Conversely, the second line integral gives:

$$\begin{aligned}\mathcal{C}(\gamma) &= \frac{m\rho_0\sigma^2}{2}\oint_\gamma d\vec{r}\cdot\Big[\hat{e}_3\wedge A_{tot}\nabla A_{tot}\Big] = \frac{m\rho_0\sigma^2}{2}A(\vec{R})\oint_\gamma d\vec{r}\cdot\big(\hat{e}_3\wedge\nabla A\big)\\ &= \frac{\rho_0\hbar}{2}A(\vec{R})\oint_\gamma d\vec{r}\cdot\vec{v}(\vec{r}) = \frac{\rho_0\hbar}{2}A(\vec{R})\bigg(-\sum_i k_i+\sum_i k_i\bigg) = 0\end{aligned} \tag{3.44}$$

where, again, the fact that $A(\vec{R}) = const$ along γ has been employed. The combination of 3.41 and 3.43 together finally produces the Hamiltonian for a disk-like obstruction:

$$\begin{aligned}\mathcal{H} &= \mathcal{C}(\Gamma) - \frac{\rho_*}{4\pi}\bigg[\frac{1}{2}\sum_i\sum_{j\neq i}k_ik_j ln\frac{|\vec{s_j}-\vec{s_i}|^2}{\lambda^2} - \frac{1}{2}\sum_i\sum_{j\neq i}k_ik_j ln\frac{|\vec{s_j}-\vec{s_i}^*|^2}{\lambda^2}\\ &\quad - \frac{1}{2}\sum_i k_i^2 ln\frac{|\vec{s_i}-\vec{s_i}^*|^2}{\lambda^2} - \frac{1}{2}\bigg(\sum_j k_j\bigg)\sum_i k_i ln\frac{|\vec{s_i}|^2}{\lambda^2}\bigg]\\ &= \mathcal{C}(\Gamma) - \frac{\rho_*}{4\pi}\bigg[\sum_i\sum_{j\neq i}k_ik_j ln\frac{|\vec{s_j}-\vec{s_i}|^2}{\lambda^2}\\ &\quad - \frac{1}{2}\sum_i\sum_j k_ik_j ln\frac{(|\vec{s_j}|^2|\vec{s_i}|^2+R^4-2R^2\vec{s_i}\cdot\vec{s_j})}{\lambda^2|\vec{s_j}|^2}\bigg]\end{aligned} \tag{3.45}$$

It has been shown indeed that

$$\mathcal{H}(\vec{r_1},..,\vec{r_n};\vec{r_1}^*,..,\vec{r_n}^*) = \mathcal{H}(\vec{s_1}^*,..,\vec{s_n}^*;\vec{s_1},..,\vec{s_n})$$

and so that the dynamical descriptions of a gas of N vortices confined in a circular trap and scattered against a disk-like obstruction are equivalent. In the simplest scenario, when $N = 2$, the previous Hamiltonian gets reduced to the one typically considered in literature [22], [2], [3] when dealing with quantum vortices:

$$\mathcal{H}_{1,2} = -\frac{\rho_*}{4\pi}\bigg[k_1k_2 ln\frac{|R^2-z_1\bar{z}_2|^2}{|R(z_1-z_2)|^2} - k_1 ln\bigg(1-\frac{|z_1|^2}{R^2}\bigg) - k_2 ln\bigg(1-\frac{|z_2|^2}{R^2}\bigg)\bigg] \tag{3.46}$$

where vector $z_j \doteq x_j + iy_j$ is such that $|z_j|^2 = |\vec{r_j}|^2$.

Dynamical equations are easily derived through the canonical Poisson Brackets with respect to canonical variables x_j, y_j such that $\{x_i, y_j\} = \delta_{ij}/(\rho_* k_i)$:

$$\begin{cases}\dot{x_j} &= \{x_j,\mathcal{H}_{1,2}\} = \frac{1}{\rho_* k_j}\frac{\partial\mathcal{H}_{1,2}}{\partial y_j}\\ \dot{y_j} &= \{y_j,\mathcal{H}_{1,2}\} = -\frac{1}{\rho_* k_j}\frac{\partial\mathcal{H}_{1,2}}{\partial x_j}\end{cases} \tag{3.47}$$

that clearly differ from the Helmoltz-Kirckhoff equations due to the profound change in the Hamiltonian that here includes a complex interaction term.

3.3 Massive Vortices and dynamics

A further generalization of the model, able to grasp more physically meaningful aspects, prescribes to incorporate the presence of massive cores: this is performed by the introduction of a Lagrangian of the form

$$\mathcal{L} = \sum_{j=1}^{2} \left[\frac{m_j}{2} \left(\dot{x_j}^2 + \dot{y_j}^2 \right) + \frac{k_j \rho_*}{2} \left(y_j \dot{x_j} - x_j \dot{y_j} \right) \right] - \mathcal{H} \tag{3.48}$$

where m_j represent the masses hosted by the $j-th$ vortex. Such *Variational Ansatz* can be properly justified by means of the so-called **Time-dependent variational Lagrangian approach** whose major details will be properly discussed in the following subsection.

In Lagrangian formalism, dynamical equation are found thanks to the well-known *Euler-Lagrange equations*: $d/dt(\partial\mathcal{L}/\partial\dot{q}_i) = 0$, $q = x, y$ and $i = 1{,}2$ for Lagrangian (3.48):

$$\begin{cases} m_1 \ddot{x_1} &= -k_1 \rho_* \dot{y_1} + \frac{\rho_* k_1}{2\pi} \left[k_2 \frac{x_1 - x_2}{|\vec{r_1} - \vec{r_2}|^2} + k_1 \frac{x_1}{R^2 - |\vec{r_1}|^2} + k_2 \frac{R^2 x_2 - |\vec{r_2}|^2 x_1}{R^4 - 2R^2 x_1 x_2 + |\vec{r_1}|^2 |\vec{r_2}|^2} \right] \\ m_1 \ddot{y_1} &= k_1 \rho_* \dot{x_1} + \frac{\rho_* k_1}{2\pi} \left[k_2 \frac{y_1 - y_2}{|\vec{r_1} - \vec{r_2}|^2} + k_1 \frac{y_1}{R^2 - |\vec{r_1}|^2} + k_2 \frac{R^2 y_2 - |\vec{r_2}|^2 y_1}{R^4 - 2R^2 y_1 y_2 + |\vec{r_1}|^2 |\vec{r_2}|^2} \right] \\ m_2 \ddot{x_2} &= -k_2 \rho_* \dot{y_2} + \frac{\rho_* k_2}{2\pi} \left[k_1 \frac{x_2 - x_1}{|\vec{r_2} - \vec{r_1}|^2} + k_2 \frac{x_2}{R^2 - |\vec{r_2}|^2} + k_1 \frac{R^2 x_1 - |\vec{r_1}|^2 x_2}{R^4 - 2R^2 x_1 x_2 + |\vec{r_1}|^2 |\vec{r_2}|^2} \right] \\ m_2 \ddot{x_2} &= +k_2 \rho_* \dot{x_2} + \frac{\rho_* k_2}{2\pi} \left[k_1 \frac{y_2 - y_1}{|\vec{r_2} - \vec{r_1}|^2} + k_2 \frac{y_2}{R^2 - |\vec{r_2}|^2} + k_1 \frac{R^2 y_1 - |\vec{r_1}|^2 y_2}{R^4 - 2R^2 y_1 y_2 + |\vec{r_1}|^2 |\vec{r_2}|^2} \right] \end{cases} \tag{3.49}$$

that in a compact vectorial formulation become:

$$m_j \ddot{\vec{r_j}} = k_j \rho_* \hat{e}_3 \wedge \dot{\vec{r_j}} + \frac{\rho_* k_j}{2\pi} \left[k_i \frac{\vec{r_j} - \vec{r_i}}{|\vec{r_j} - \vec{r_i}|^2} + k_j \frac{\vec{r_j}}{R^2 - |\vec{r_j}|^2} + k_i \frac{R^2 \vec{r_i} - |\vec{r_i}|^2 \vec{r_j}}{R^4 - 2R^2 \vec{r_i} \vec{r_j} + |\vec{r_i}|^2 |\vec{r_j}|^2} \right] \tag{3.50}$$

It is interesting to observe that in the limit $R \to 0$ or more precisely $|\vec{r_i}|, |\vec{r_j}| \gg R$, meaning that the size of the obstacle is vanishingly small, one restores the dynamical equations describing a gas of N free *massive* vortices. Indeed in this limit Lagrangian (3.48) loses the contribution of the boundary coming from $\mathcal{H}$, leading to:

$$\begin{cases} m_1 \ddot{x_1} &\simeq -k_1 \rho_* \dot{y_1} + \frac{\rho_* k_1}{2\pi} \left[k_2 \frac{x_1 - x_2}{|\vec{r_1} - \vec{r_2}|^2} \right] \\ m_1 \ddot{y_1} &\simeq k_1 \rho_* \dot{x_1} + \frac{\rho_* k_1}{2\pi} \left[k_2 \frac{y_1 - y_2}{|\vec{r_1} - \vec{r_2}|^2} \right] \\ m_2 \ddot{x_2} &\simeq -k_2 \rho_* \dot{y_2} + \frac{\rho_* k_2}{2\pi} \left[k_1 \frac{x_2 - x_1}{|\vec{r_2} - \vec{r_1}|^2} \right] \\ m_2 \ddot{y_2} &\simeq k_2 \rho_* \dot{x_2} + \frac{\rho_* k_2}{2\pi} \left[k_1 \frac{y_2 - y_1}{|\vec{r_2} - \vec{r_1}|^2} \right] \end{cases} \tag{3.51}$$

where it has been assumed $k_1 = -k_2$ as the two vortices are part of a vortex-antivortex dipole. In the following chapter, the massive vortex dynamics will be

simulated numerically by means of the software *Wolfram Mathematica* to study the scattering of a dipole against a circular obstacle.

3.3.1 Time-dependent Variational Lagrangian Method

This methodology is widely employed in non-linear problems and is particularly useful in three-dimensional problems where numerical simulations are computationally expensive. Indeed it is worth mentioning that, despite the dynamics in object evolves in a two-dimensional domain, the dynamics is originally three-dimensional. Due to the regime of interaction considered the condensate is almost compressed on a 2D disk leading to a dynamics that is essentially planar due to the negligible elongation of the system along its vertical component. Although not exact, this technique is a good qualitative approach that allows to find approximated but analytical results for a complex system.

First recall that a Bose-Einstein Condensate at zero temperature is described within the *Non-linear Schröedinger Equation* (NLSE):

$$i\hbar\frac{\partial\psi}{\partial t} = -\frac{\hbar^2}{2m}\nabla^2\psi + V(\vec{r})\psi + U_0|\psi|^2\psi \tag{3.52}$$

where $V(\vec{r})$ is the trapping potential and $U_0 = 4\pi\hbar^2 a/m$ is the effective interaction potential as a result of Bogoliubov theory [16], [18], with a the scattering length. Considering an harmonically-trapped BEC, the expression of its confining potential reads:

$$V(\vec{r}) = \frac{1}{2}m\omega^2\left(\lambda_x^2x^2 + \lambda_y^2y^2 + \lambda_z^2z^2\right)$$

The basic idea behind the variational method is to take a trial function with a fixed shape, but with some free (time-dependent) parameters. On the practical level the TDVL method bypasses the Gross-Pitaevskii equation and limits the dynamics on a finite set of time-dependent *variational parameters*, by introducing **Variational Ansatz**: it consists in assuming that in the specific regime where interactions are weak enough, the Gaussian shape of the exact solution (where $g = 0$) is almost unaltered. Thus one assumes that:

$$\psi(x,y,z,t) = A(t)\prod_{\eta=x,y,z} exp\left[-\frac{(\eta-\eta_0(t))^2}{2\omega_\eta^2} + i\eta\alpha_\eta(t) + i\eta^2\beta_\eta(t)\right] \tag{3.53}$$

where $\omega \ll |\vec{r_i} - \vec{r_j}|$. It comes useful to notice that all such parameters possess a physical meaning and directly influence many relevant quantities. Indeed the velocity of the Gaussian wavepacket linearly depends on α:

$$\vec{v}(t) = \frac{\langle\psi|\hat{v}|\psi\rangle}{\langle\psi|\psi\rangle} = \frac{\hbar}{m}\vec{\alpha}(t)$$

while its width on ω:

$$(\Delta x)^2 = \frac{\langle\psi|(x - x_0(t))^2|\psi\rangle}{\langle\psi|\psi\rangle} = \frac{(\omega_x(t))^2}{2}$$

The amplitude $A(t)$ on the other side is found by imposing the normalization condition on the trial wavefunction and reads:

$$A(t) = \left[\frac{N}{\pi^{3/2}\prod_{\eta=x,y,z}\omega_\eta(t)}\right]^{1/2}$$

So while α can be recasted as a slope, parameter β as a (curvature)$^{-1/2}$.

On the other side, this methodology allows to study the *collective mode dynamics* of the condensate, by analyzing dynamical equations for the variational parameters. Concerning the center of the condensate E-L provides:

$$\ddot{\eta_0} + \lambda_\eta^2\nu^2\eta_0 = 0, \quad \eta = x, y, z \tag{3.54}$$

showing how it oscillates harmonically with frequencies $\lambda_\eta\nu$ and forming the so-called *dipole mode*. It is important to observe how in this particular choice of trapping potential, the motion does not depend on the number of particles, and therefore it is not affected by non-linear effects. As a result the center of mass of the condensate responds like a classical particle to the external potential. Concerning the width $\Delta x \sim \omega_x$, its dynamics is ruled by:

$$\ddot{\omega}_x + \lambda_x^2\nu^2\omega_x = \frac{\hbar^2}{m^2\omega_x^3} + \sqrt{\frac{2}{\pi}}\frac{a\hbar^2 N}{m^2\omega_x^2\omega_y\omega_z} \tag{3.55}$$

and similarly for the other components. Then the remaining variational parameters can be trivially determined through the center's coordinates and the widths by means of the relations:

$$\beta_\eta = -\frac{m\dot{\omega}_\eta}{2\hbar^2\omega_\eta}, \quad \alpha_\eta = -\frac{m\dot{\eta}_0}{\hbar^2} - 2\beta_\eta\eta_0 \tag{3.56}$$

The investigation of the collective mode dynamics leads to important results concerning the expansion/contraction dynamics of the condensate and its oscillatory behaviour, through the solution of the equation for variational parameter ω_η.

In this context, as provided in the work [2], a two-component dilute Bose-Einstein condensate is considered and so the overall system's wavefunction can be seen as a superposition of ψ_a representing the wave function of the a-component that contains the vortices and ψ_b, the wavefunction of the component trapped in the vortex

cores. In this regard the authors applied the methodology outlined in [20] to the b-component. From the lagrangian viewpoint, the dynamics of N_v classical massive vortices is accounted by the following Lagrangian (referring to the a-component)

$$L_a = \sum_{j=1}^{N_v} \frac{1}{2} M_j \, \dot{\vec{r}}_j^{\,2} + \sum_{j=1}^{N_v} \pi n \hbar q_j \vec{r}_j \times \vec{r}_j \dot{\hat{z}} - E(\vec{r_1}, ..., \vec{r_n}) \tag{3.57}$$

where aside from the Newtonian kinetic term, the central contribution, familiar in the Lagrangian of a set of charged particles in presence of electromagnetic potentials, involves velocity and position. The potential energy can be seen as the contribution of both the interaction energy of vortex $\vec{r_j}$ with its virtual image on the boundary (Φ_j) and the interaction energy of vortices $\vec{r_j}$ and $\vec{r_k}$ (V_{jk}), thus resulting in $E = \sum_j \Phi_j + \sum_j V_{jk}$. For the present problem the variational Ansatz (3.53) will be slightly adjusted as follows:

$$\psi_b(x, y, z, t) = \sum_{i=1}^{N_v} \left(\frac{N_b}{N_v \pi \sigma^2} \right)^{\frac{1}{2}} exp\left[- \frac{|\vec{r} - \vec{r_j}(t)|^2}{2\sigma^2} + i\vec{r} \cdot \vec{\alpha_j}(t) \right] \tag{3.58}$$

describing a Gaussian wavepacket with linear phase $\vec{r} \cdot \vec{\alpha_j}$, with b-component cores small due to condition $\sigma \ll |\vec{r_i} - \vec{r_k}|$. At this point the TDVL method involves the substitution of Ansatz (3.58) inside the Lagrangian functional, since solving the NLSE (3.52) can be recasted as the minimization of the action related to the Lagrangian:

$$L[\psi] = \int d^3\vec{r} \left[\left(\psi^* \frac{\partial \psi}{\partial t} - \frac{\partial \psi^*}{\partial t} \psi \right) - \frac{\hbar^2}{2m} |\nabla \psi|^2 + V(\vec{r}) |\psi|^2 + \frac{g}{2} |\psi|^4 \right] \tag{3.59}$$

After some algebra, the system can be traced back to a Lagrangian that now depends on the aforementioned variational parameters, meaning that:

$$L[\psi] = T[\psi] - E[\psi] \rightarrow L\big(\vec{r}(t), \dot{\vec{r}}(t), \vec{\alpha}(t), \dot{\vec{\alpha}}(t)\big) \tag{3.60}$$

from which, by means of Euler-Lagrange equations, dynamical equations for such parameters are of trivial derivation. In particular, noticing that ψ_b is a localized wavepacket centered in $\vec{r_j}(t)$ and moving with velocity $\dot{\vec{r}}_j(t) = \hbar \vec{\alpha_j} / m_b$, it is possible to find the following expression:

$$\begin{aligned} L_b &= - \sum_{j=1}^{N_v} \frac{N_b}{N_v} \left(\hbar \vec{r_j} \cdot \dot{\vec{\alpha}}_j + \frac{\hbar^2}{2m_b} \vec{\alpha_j}^{\,2} \right) \\ &= \frac{N_b}{N_v} \sum_{j=1}^{N_v} \left[\frac{m_b}{2} \, \dot{\vec{r}}_j^{\,2} - \frac{\hbar^2}{2m_b} \big(\vec{\alpha_j} - \frac{m_b}{\hbar} \dot{\vec{r}}_j \big)^2 \right] \\ &= \sum_{j=1}^{N_v} \frac{1}{2} M_c \, \dot{\vec{r}}_j^{\,2} = \sum_{j=1}^{N_v} \frac{M_b}{2N_v} \, \dot{\vec{r}}_j^{\,2} \end{aligned} \tag{3.61}$$

where $M_c = N_b m_b / N_v = M_b / N_v$, with N_v is the number of point vortices. The second equality in previous equation follows from noticing that, since neglecting a total time derivative doesn't alter the resulting equations, the term $\vec{r}_j \cdot \dot{\vec{\alpha}}_j$ becomes $-\dot{\vec{r}}_j \cdot \vec{\alpha}_j + d(\vec{r}_j \cdot \vec{\alpha}_j)/dt$ apart from the total time derivative.

The combination of the previous result for L_b together with the L_a variational Lagrangian provide the assumed model Lagrangian (3.57), proving the effectiveness of the discussed variational method.

Chapter 4

Algebraic Description

> "By believing passionately in something that still does not exist, we create it. The nonexistent is whatever we have not sufficiently desired."
>
> Franz Kafka

A different perspective on the the description of the dynamical behaviour of quantum vortices has been outlined in [19] where, by means of a group-theoretical approach, the system has been classified in a specific algebraic framework thanks to its symmetries and conserved quantities. Such a description is strongly based on the field-theoretical formulation of the system and mainly focus on the concept of symmetries and how they relate to conservation laws. Indeed the location of a dynamical system into a precise algebraic structure allows not only to find its (eventual) symmetries but also, in virtue of *Noether's Theorem*, to identify its (eventual) conserved quantities, a crucial step in understanding the system's behaviour.

Nevertheless, the **integrability character** of the model drastically changes when accounting for the presence of massive cores, strongly limiting the analytical approaches to its investigation. Their inclusion infact leads to the increase of the overall dynamical variables resulting in a system with 8 degrees of freedom contrary to the only 4 present in the massless scenario. This complication will be bypassed analyzing the asymptotic regimes where the influence of the boundary can be neglected allowing to restore 2 conservation laws related to the translational symmetries along the x, y-axis.

After a brief discussion on a few important topics in Classical Mechanics, an inspiring algebraic approach to the (massless) disk-pair system will be presented and extended to the massive scenario. Despite the lack of complete integrability, the system doesn't appear to be chaotic. Indeed *KAM Theorem* points out how non-integrable systems do not automatically lead to chaotic dynamics. Aside from the transient regime with the high non-linear interaction with the obstacle, the dipole will be shown to present some important conservation laws that suggest an overall stable character, subsequently confirmed by numerical simulations.

4.1 General Aspects of Analytical Mechanics

Poisson Brackets represent a powerful instrument when dealing with Hamiltonian dynamics: not only they are deeply linked with Hamilton's equations, but they also provide a straigthforward way to find conserved quantities. Moreover they are deeply related to *Noether's Theorem*, which basically states that for every *continuous symmetry* of the action of a physical system, there exists a corresponding *conserved quantity* Q called **Noether Charge**. Invariance under specific transformations implies then the emergence of the associated conserved Noether Charges.

The set of all symmetries of a dynamical system that can be composed and inverted forms a group, called the *Symmetry Group* of the system, where each element corresponds to a specific symmetry transformation. For continuous symmetries, the symmetry group is often a *Lie Group*, where the infinitesimal generators of these transformations form a *Lie Algebra*, encoding the structure of the symmetry transformations. The conserved quantities correspond to the generators of the symmetry transformations in the Lie Algebra.

For the specific case, the following sections will rely on a methodology based on the concept of *dynamical algebra* [19], [4], a Lie Algebra closed under commutation. Such closure property means that the commutator of any two algebra elements is still an element of the algebra. Since a Lie Algebra is uniquely determined once all commutators $[\hat{e}_j, \hat{e}_k] = i \sum_m f_{jkm} \hat{e}_m$ are given (recalling that $\hat{e}_1, \hat{e}_2, ..., \hat{e}_n$ are the generators of its corresponding n-dimensional vector space), then a model Hamiltonian $\hat{\mathcal{H}}$ belongs to a specific dynamical algebra $\mathcal{A}$ whenever it can be expressed as a linear combination of the algebra's generators. Operatively:

$$\hat{\mathcal{H}} = \sum_j h_j \hat{e}_j$$

This allows to identify conserved quantities with algebra's invariants but also to provide a trivial diagonalization of sub-Hamiltonians $\hat{H}_k$, assuming the separability of Hamiltonian $\hat{\mathcal{H}} = \sum_k \hat{H}_k$.

4.1.1 Integrability of dynamical systems and chaos

An important tool that comes into play when dealing with a dynamical system is the concept of **integrability**: ad dynamical system is said to be integrable if it possesses enough conserved quantities (integrals of motion) to allow the system's equations of motion to be solved exactly, typically by quadratures.

Formally, for a system with n degrees of freedom (with a $2n$-dimensional phase space) described by a Hamiltonian $H(q_i, p_i)$, the system is said to be **Liouville Integrable** [5] if there exist n independent conserved quantities

$$\{\mathcal{H}, F_i\} = 0, \quad 1 = 1, ..., n$$

(often called first integrals) *in involution*:

$$\{F_i, F_j\} = 0, \quad \forall i, j$$

On the practical level, the integrability property of a system allows its description in terms of its conserved quantities: thanks to Noether's theorem infact, if the system possess n symmetries and so n conserved quantities that are in involution, then it is integrable. This condition often allows to find analytical solutions, contrary to generic dynamical systems for which the lack of a sufficient number of prime integrals prevents from finding exact solutions. Despite **chaotic systems** are not-integrable, not all systems that lack of complete integrability are chaotic since they may exhibit regular or quasi-periodic motions that may be stable over time. Infact in order to be defined *chaotic*, a system must possess high sensitivity to initial conditions, typically measured by means of the *Lyapunov exponent*. In this regard an important result is given by *KAM Theorem* (Kolmogorov-Arnold-Moser) which describes indeed how, under certain conditions, non-integrable systems that are "close" to integrable ones can still exhibit quasi-periodic motion on tori (which is regular and not chaotic) showing that non-integrable systems do not automatically lead to chaos.

4.2 The Scattering Model of a Vortex Pair

A dynamical-algebra approach to the study of Vortex Quantum Dynamics (VQD) completely relying on the algebraic characterization of the system has been performed by V. Penna [19], where it has been considered the case of two massless vortices with different combination of vorticity fields scattered against a circular obstacle. Such VQD has been studied by means of the so called *spectrum generating algebra method*, consisting in the identification of a complete set of generators forming a Lie Algebra (the dynamical algebra). Prime integrals of the system then naturally arise from algebra's invariants, typically expressed as linear combinations of the generators.

4.2.1 Mass-less case

Recall then the Hamiltonian of N free point-like vortices in a frictionless fluid 3.11

$$\mathcal{H}(\vec{r_1},...,\vec{r_n}) = -\frac{\rho}{4\pi}\sum_{i\neq j} k_i k_j ln\left(\frac{|\vec{r_i}-\vec{r_j}|}{\lambda}\right)$$

and canonical Poisson Brackets

$$\{x_i, y_j\} = \frac{\delta_{ij}}{\rho k_j}$$

where momenta $p_{x_j} = \rho k_j x_j$ and $p_{y_j} = \rho k_j y_j$ has been introduced, fulfilling $[x_i, p_j] = i\hbar\delta_{ij}$.

It has been shown that:

$$J_x = \rho\sum_m k_m x_m \tag{4.1}$$

$$J_y = \rho\sum_m k_m y_m \tag{4.2}$$

$$J_z = -\frac{\rho}{2}\sum_m k_m(x_m^2 + y_m^2) \tag{4.3}$$

respectively the *generator of translations along x-axis*, the *generator of translations along y-axis*, and the *generator of rotations* fulfill the equation

$$-\rho J_* = 2CJ_z + J_x^2 + J_y^2$$

where J_* is the analogue of the *Casimir operator* and has the form

$$J_* = \frac{\rho}{2}\sum_{i\neq j} k_i k_j[(x_i - x_j)^2 + (y_i - y_j)^2]$$

and $C = \rho\sum_j k_j$ stands for the total vorticity. Most importantly, such generators are constants of motion, indeed satisfying, for $a = x, y, z$, relations:

$$\{J_a, J_*\} = 0, \quad \{\mathcal{H}, J_a\} = \{\mathcal{H}, J_*\} = 0 \tag{4.4}$$

$$\{J_x, J_y\} = C, \quad \{J_z, J_x\} = J_y, \quad \{J_y, J_z\} = J_x \tag{4.5}$$

showing how they suitably represent generators of the $e(2)$-like algebra, in the light of the closedness property. The author showed how in the case of $N = 2$ vortices, for $k_1, k_2 > 0$ they rotate along concentric circumferences which collapse into a

single circular orbit for $k_1 \to k_2$. When $k_1 \to -k_2$ the full VA-regime emerges, seeing the pair running along straight parallel lines. The system is indeed completely integrable as the number of conserved quantities overtakes the number of degrees of freedom, given only by the vortices' positions.

When accounting for the presence of the circular obstacle (see section 3.2.1) one should recall that the system's Hamiltonian changes, becoming

$$\mathcal{H}_{1,2} = -\frac{\rho_*}{4\pi}\left[k_1 k_2 ln\frac{|R^2 - z_1\bar{z}_2|^2}{|R(z_1 - z_2)|^2} - k_1 ln\left(1 - \frac{|z_1|^2}{R^2}\right) - k_2 ln\left(1 - \frac{|z_2|^2}{R^2}\right)\right]$$

but despite the system loses 2 conserved quantities in the light of the fact that the obstacle prevents from keeping translational symmetries along $x, y - axis$, the integrability character is maintained allowing to adopt a fully analytical approach. The author showed infact that, introducing $D^2 = |\vec{r_1} - \vec{r_2}|^2$, it is possible to find 4 conserved quantities (different from the previous ones) that in the VV-pair case can be identified with the generators of $su(2)$ algebra, while the VA-pair gets approached within the $su(1,1)$ algebraic scheme.

The VA-pair scenario possesses a limiting case when $k_2 \to -k_1$: a transition takes place from a confined behaviour where the trajectories are represented by circumferences to a situation where the pair freely drifts away in the plane. This appealing results suggest that the disk-pair dynamics could be suitably reformulated in terms of a generalized angular momentum dynamics. The main difference between VV and VA dynamics seems to stand in the energetic disadvantage of the former as a consequence of vorticity accumulation. The VA-pair on the contrary appears much more stable because of the proper balance induced by the opposite circulation fields.

4.2.2 Massive case

When accounting for the presence of massive cores the situation drastically changes: the emergence of new degrees of freedom embodied by the masses lead to the loss of the system's integrability. The number of $d.o.f.$ (now 8) overtakes the number of prime integrals (2) and the system can no longer be described in terms of its conserved quantities, requiring then a different approach with respect to the one previously adopted. Assuming that the non-linear interaction effects induced by the obstacle are exhausted at finite distance, it seems reasonable to postulate the existence of an *asymptotic regime* where the vortex pair behaves undisturbed. This means that way before encountering the obstacle and way after its collision, the system should be modelled by the original Hamiltonian describing free vortices

(3.11). These two regions are marked by condition $R \ll |\vec{r_i}|, |\vec{r_j}|$ stating that the vortices' positions are (in modulus) way bigger than the obstacle's radius and so that such vortices are located far from it. The original dynamical equations (3.49) get approximated as follows:

$$\begin{cases} m_1 \ddot{\boldsymbol{x_1}} & \simeq -k_1 \rho_* \dot{\boldsymbol{y_1}} + \frac{\rho_* k_1}{2\pi} \left[k_2 \frac{\boldsymbol{x_1} - \boldsymbol{x_2}}{|\vec{r_1} - \vec{r_2}|^2} \right] \\ m_1 \ddot{\boldsymbol{y_1}} & \simeq k_1 \rho_* \dot{\boldsymbol{x_1}} + \frac{\rho_* k_1}{2\pi} \left[k_2 \frac{\boldsymbol{y_1} - \boldsymbol{y_2}}{|\vec{r_1} - \vec{r_2}|^2} \right] \\ m_2 \ddot{\boldsymbol{x_2}} & \simeq -k_2 \rho_* \dot{\boldsymbol{y_2}} + \frac{\rho_* k_2}{2\pi} \left[k_1 \frac{\boldsymbol{x_2} - \boldsymbol{x_1}}{|\vec{r_2} - \vec{r_1}|^2} \right] \\ m_2 \ddot{\boldsymbol{y_2}} & \simeq k_2 \rho_* \dot{\boldsymbol{x_2}} + \frac{\rho_* k_2}{2\pi} \left[k_1 \frac{\boldsymbol{y_2} - \boldsymbol{y_1}}{|\vec{r_2} - \vec{r_1}|^2} \right] \end{cases} \tag{4.6}$$

Various experimental observations suggest that in such asymptotic regimes acceleration terms should be negligible since the velocities remain constant in terms of modulus and direction aside from the region surrounding the obstacle. Thanks to this observation, previous equations get rewritten as:

$$\begin{cases} \dot{\boldsymbol{x_1}} & \simeq -\frac{k_2}{2\pi} \frac{\boldsymbol{y_1} - \boldsymbol{y_2}}{|\vec{r_1} - \vec{r_2}|^2} \\ \dot{\boldsymbol{y_1}} & \simeq \frac{k_2}{2\pi} \frac{\boldsymbol{x_1} - \boldsymbol{x_2}}{|\vec{r_1} - \vec{r_2}|^2} \\ \dot{\boldsymbol{x_2}} & \simeq -\frac{k_1}{2\pi} \frac{\boldsymbol{y_2} - \boldsymbol{y_1}}{|\vec{r_2} - \vec{r_1}|^2} \\ \dot{\boldsymbol{y_2}} & \simeq \frac{k_1}{2\pi} \frac{\boldsymbol{x_2} - x_1}{|\vec{r_2} - \vec{r_1}|^2} \end{cases} \tag{4.7}$$

perfectly reproducing the Helmoltz-Kirkchoff equations for massless vortices. Interestingly then, considering the system far from the influence of the obstacle seems to allow for its reduction to a specific *dynamical sub-regime* of *lightweight vortices* where the mass does not play an important role. Helpful insights in the system's dynamics are given by means of a perturbative expansion, that provides a more rigorous method to validate the set of equations 4.7.
Expressing then spatial coordinates as:

$$\boldsymbol{x_j} \simeq X_j + \epsilon x_j + o(\epsilon^2) \tag{4.8}$$

$$\boldsymbol{y_j} \simeq Y_j + \epsilon y_j + o(\epsilon^2) \tag{4.9}$$

where the zero-order term corresponds to the basic approximation and the first-order correction depends respectively on the perturbative parameter $\epsilon \ll 1$. For the first equation of the set (4.6) one obtains:

$$\begin{aligned} & m_1 \ddot{\boldsymbol{x_1}} \simeq -k_1 \rho_* \dot{\boldsymbol{y_1}} + \frac{\rho_* k_1}{2\pi} \left[k_2 \frac{\boldsymbol{x_1} - \boldsymbol{x_2}}{|\vec{\boldsymbol{r_1}} - \vec{\boldsymbol{r_2}}|^2} \right] \\ & m_1 \big(\ddot{X}_1 + \epsilon \ddot{x}_1 \big) \simeq -k_1 \rho_* \big(\dot{Y}_1 + \epsilon \dot{y_1}^{(1)} \big) + \frac{\rho_* k_1 k_2}{2\pi} \frac{\big(X_1 - X_2\big) + \epsilon \big(x_1 - x_2\big)}{|\vec{\boldsymbol{r_1}} - \vec{\boldsymbol{r_2}}|^2} \end{aligned} \tag{4.10}$$

and since

$$\begin{aligned}|\vec{\boldsymbol{r_1}} - \vec{\boldsymbol{r_2}}|^2 &\simeq \Big[\big(X_1 - X_2\big) + \epsilon\big(x_1 - x_2\big)\Big]^2 + \Big[\big(Y_1 - Y_2\big) + \epsilon\big(y_1 - y_2\big)\Big]^2 \\ &\simeq \big(X_1 - X_2\big)^2 + \big(Y_1 - Y_2\big)^2 + 2\epsilon\big(X_1 - X_2\big)\big(x_1 - x_2\big) + o(\epsilon^2) \\ &\quad + 2\epsilon\big[\big(Y_1 - Y_2\big)\big(y_1 - y_2\big) + o(\epsilon^2) \\ &= |\vec{R_1} - \vec{R_2}|^2 + 2\epsilon\big(\vec{R_1} - \vec{R_2}\big) \cdot \big(\vec{r_1} - \vec{r_2}\big) + o(\epsilon^2)\end{aligned} \tag{4.11}$$

where $\vec{R}_i$ refers to the zero-order contribution of vector $\vec{\boldsymbol{r_i}}$, meaning that $\vec{R}_i = \vec{\boldsymbol{r_i}}^{(0)} = X_i^2 + Y_i^2$, while $\vec{r_i} = \vec{\boldsymbol{r_i}}^{(1)}$ is its first-order correction. Exploiting the Taylor's expansion of the fraction in (4.10) and defining $\Delta = \big[(X_1 - X_2)(x_1 - x_2) + (Y_1 - Y_2)(y_1 - y_2)\big]$

$$\begin{aligned}\frac{1}{|\vec{\boldsymbol{r_1}} - \vec{\boldsymbol{r_2}}|^2} &\simeq \frac{1}{|\vec{R_1} - \vec{R_2}|^2 + 2\epsilon\Delta} = \frac{1}{|\vec{R_1} - \vec{R_2}|^2\big(1 + 2\epsilon\Delta/|\vec{R_1} - \vec{R_2}|^2\big)} \\ &\simeq \frac{1}{|\vec{R_1} - \vec{R_2}|^2} - \frac{2\epsilon\Delta}{|\vec{R_1} - \vec{R_2}|^4} + o(\epsilon^2) \\ &= \frac{1}{|\vec{R_1} - \vec{R_2}|^2} - \frac{2\epsilon\big[(X_1 - X_2)(x_1 - x_2) + (Y_1 - Y_2)(y_1 - y_2)\big]}{|\vec{R_1} - \vec{R_2}|^4} + o(\epsilon^2)\end{aligned} \tag{4.12}$$

where second-order corrections have been neglected. Finally, separating zero-order terms from first-order contributions one finds two distinct dynamical equations:

$$\begin{cases} m_1\ddot{X}_1 \simeq -k_1\rho_*\dot{Y}_1 + \frac{\rho_* k_1 k_2}{2\pi}\frac{X_1 - X_2}{|\vec{R_1} - \vec{R_2}|^2} \\ m_1\ddot{x}_1 \simeq -k_1\rho_*\dot{y}_1 + \frac{\rho_* k_1 k_2}{2\pi}\left[\frac{\big(x_1 - x_2\big)}{|\vec{R_1} - \vec{R_2}|^2} - \frac{2\big((X_1 - X_2)(x_1 - x_2) + (Y_1 - Y_2)(y_1 - y_2)\big)}{|\vec{R_1} - \vec{R_2}|^4}(X_1 - X_2)\right] \end{cases} \tag{4.13}$$

and observing once again that it is possible to assume the acceleration of the "bulk" term as negligible $\ddot{X}_1 \simeq 0$ due to experimental observation, the first equation concerning the zero-order term of the perturbative expansion is in perfect agreement with its corresponding equation in set (4.7):

$$\dot{Y}_1 \simeq \frac{k_2}{2\pi}\frac{X_1 - X_2}{|\vec{R_1} - \vec{R_2}|^2} \tag{4.14}$$

Thus this shows that the "bulk" dynamics addressed in the zero-order approximation is indeed stable under perturbations. Conversely the dynamics concerning the first-order contribution is linear in perturbations $\epsilon \ll 1$, proving to be negligible

in the overall dynamics of the system when considering the asymptotic regimes. Overall, the dynamics of vortex 1 is ruled by the following equations of motion:

$$\begin{cases} \dot{X}_1 = -\frac{k_2}{2\pi}\frac{Y_1 - Y_2}{|\vec{R_1} - \vec{R_2}|^2} \\ \dot{Y}_1 = \frac{k_2}{2\pi}\frac{X_1 - X_2}{|\vec{R_1} - \vec{R_2}|^2} \end{cases} \tag{4.15}$$

together with the first-order correction describing the oscillatory dynamics:

$$\begin{cases} m_1\ddot{x_1} \simeq -k_1\rho_*\dot{y_1} + \frac{\rho_* k_1 k_2}{2\pi}\left[\frac{(x_1 - x_2)}{|\vec{R_1} - \vec{R_2}|^2} - \frac{2\Big((X_1 - X_2)(x_1 - x_2) + (Y_1 - Y_2)(y_1 - y_2)\Big)}{|\vec{R_1} - \vec{R_2}|^4}(X_1 - X_2)\right] \\ m_1\ddot{y_1} \simeq k_1\rho_*\dot{x_1} + \frac{\rho_* k_1 k_2}{2\pi}\left[\frac{(y_1 - y_2)}{|\vec{R_1} - \vec{R_2}|^2} - \frac{2\Big((X_1 - X_2)(x_1 - x_2) + (Y_1 - Y_2)(y_1 - y_2)\Big)}{|\vec{R_1} - \vec{R_2}|^4}(Y_1 - Y_2)\right] \end{cases} \tag{4.16}$$

Similar considerations and calculations concern the second vortex, whose dynamics is governed by:

$$\begin{cases} \dot{X}_2 = -\frac{k_1}{2\pi}\frac{Y_2 - Y_1}{|\vec{R_2} - \vec{R_1}|^2} \\ \dot{Y}_2 = \frac{k_1}{2\pi}\frac{X_2 - X_1}{|\vec{R_2} - \vec{R_1}|^2} \end{cases} \tag{4.17}$$

jointly with

$$\begin{cases} m_2\ddot{x_2} \simeq -k_2\rho_*\dot{y_2} + \frac{\rho_* k_2 k_1}{2\pi}\left[\frac{(x_2 - x_1)}{|\vec{R_2} - \vec{R_1}|^2} - \frac{2\Big((X_2 - X_1)(x_2 - x_1) + (Y_2 - Y_1)(y_2 - y_1)\Big)}{|\vec{R_2} - \vec{R_1}|^4}(X_2 - X_1)\right] \\ m_2\ddot{y_2} \simeq k_2\rho_*\dot{x_2} + \frac{\rho_* k_2 k_1}{2\pi}\left[\frac{(y_2 - y_1)}{|\vec{R_2} - \vec{R_1}|^2} - \frac{2\Big((X_2 - X_1)(x_2 - x_1) + (Y_2 - Y_1)(y_2 - y_1)\Big)}{|\vec{R_2} - \vec{R_1}|^4}(Y_2 - Y_1)\right] \end{cases} \tag{4.18}$$

Resulting motion equations require a careful discussion: assuming the validity of eq. 4.7, valid in the asymptotic regimes, requires their compatibility with 4.6. For this to be true, the asymptotic dynamics described by the Helmoltz-Kirchoff must be compatible with the request $\ddot{x_i} = \ddot{y_i} = const \equiv 0$ for $i = 1{,}2$. This is indeed verified whenever $\dot{x_i} = \dot{y_i} = const$, representing a constraint on the dynamical evolution of the system, satisfied only if $\boldsymbol{y_i} - \boldsymbol{y_j} = \boldsymbol{x_i} - \boldsymbol{x_j} = const$. The fact that the role of the masses loses its importance is a then a consequence of postulating the existence of specific sub-regimes where the following conditions are constantly verified:

$$\begin{aligned} \boldsymbol{y_1} - \boldsymbol{y_2} = const \Rightarrow \dot{\boldsymbol{x_1}} = \dot{\boldsymbol{x_2}} = const \Rightarrow \ddot{\boldsymbol{x_1}} = \ddot{\boldsymbol{x_2}} \equiv 0 \\ \boldsymbol{x_1} - \boldsymbol{x_2} = const \Rightarrow \dot{\boldsymbol{y_1}} = \dot{\boldsymbol{y_2}} = const \Rightarrow \ddot{\boldsymbol{y_1}} = \ddot{\boldsymbol{y_2}} \equiv 0 \end{aligned} \tag{4.19}$$

where the fact that $\dot{\boldsymbol{x_1}} = \dot{\boldsymbol{x_2}}$ together with $\dot{\boldsymbol{y_1}} = \dot{\boldsymbol{y_2}}$ has been noticed as directly coming from 4.7 since $k_1 = -k_2$. The results coming from this methodology state then whenever the distancing between the vortices is kept constant their respective velocities remain so, resulting in a uniform motion (e.g. with zero accelerations)

resembling the trivial dynamics of *free massless vortices*.

Another interesting perspective can be considered when accounting for the system's conserved quantities. In such asymptotic regimes where the influence of the obstacle is negligible, translational symmetries along $x, y - axis$ are gained. Such generators differ from the ones concerning the massless scenario, and read:

$$\mathcal{J}_x \doteq \sum_j \left(p_{x_j} + \rho_* \frac{k_j}{2} y_j \right) = \sum_j \left(m_j \dot{x}_j + \rho_* k_j y_j \right) \tag{4.20}$$

$$\mathcal{J}_y \doteq \sum_j \left(p_{y_j} - \rho_* \frac{k_j}{2} x_j \right) = \sum_j \left(m_j \dot{y}_j - \rho_* k_j x_j \right) \tag{4.21}$$

$$\begin{aligned} \mathcal{J}_z &\doteq \sum_j \left[\frac{\rho_*}{2} \left(x_j^2 + y_j^2 \right) + \left(x_j p_{y_j} - y_j p_{x_j} \right) \right] \\ &= \sum_j \left[m_j \left(x_j \dot{y}_j - y_j \dot{x}_j \right) - \rho_* \frac{k_j}{2} \left(x_j^2 + y_j^2 \right) \right] \end{aligned} \tag{4.22}$$

where momenta $p_{x_j} = m_j \dot{x}_j + \rho_* k_j y_j / 2$ and $p_{y_j} = m_j \dot{y}_j - \rho_* k_j x_j / 2$ are now the standard ones. To begin one should prove that such generators are indeed prime integrals by evaluating the corresponding Poisson Bracket against the Hamiltonian. For the generator along the x-axis one finds:

$$\begin{aligned} \dot{\mathcal{J}}_x &= \{ \mathcal{J}_x, \mathcal{H} \} = \{ p_{x_1} + p_{x_2}, \mathcal{H} \} + \rho_* \frac{k_1}{2} \{ y_1, \mathcal{H} \} + \rho_* \frac{k_2}{2} \{ y_2, \mathcal{H} \} \\ &= -\frac{\partial \mathcal{H}}{\partial x_1} - \frac{\partial \mathcal{H}}{\partial x_2} + \rho_* \frac{k_1}{2} \dot{y}_1 + \rho_* \frac{k_2}{2} \dot{y}_2 = \rho_* \frac{k_1 k_2}{4\pi} \frac{x_1 - x_2}{|\vec{r_1} - \vec{r_2}|^2} + \rho_* \frac{k_1 k_2}{4\pi} \frac{x_2 - x_1}{|\vec{r_2} - \vec{r_1}|^2} \\ &+ \rho_* \frac{k_1}{2} \left(\frac{k_2}{2\pi} \frac{x_1 - x_2}{|\vec{r_1} - \vec{r_2}|^2} \right) + \rho_* \frac{k_2}{2} \left(\frac{k_1}{2\pi} \frac{x_2 - x_1}{|\vec{r_2} - \vec{r_1}|^2} \right) = 0 \end{aligned} \tag{4.23}$$

where in the last equivalence asymptotic equations (4.7) have been employed. Moreover by observing that $(x_1 - x_2) = -(x_2 - x_1)$, it has been proved that $\dot{\mathcal{J}}_x = 0$. Similar calculations are performed for other generators.

In conclusion, the approach adopted so far consisted in neglecting the transient regime where the vortex dipole interact with the obstacle and the loss of integrability prevents from approaching the system in an exact, analytical way. In the so called *asymptotic regimes*, indicated by the condition $R \ll |\vec{r_j}|$, despite the system is still not completely integrable, the emergence of previously lost conserved quantities may shed a light in further understanding such complex interaction dynamics. From the aforementioned generators it is possible to find 3 conservation

laws by imposing, respectively: $\mathcal{J}_{x_{in}} = \mathcal{J}_{x_{out}}$, $\mathcal{J}_{y_{in}} = \mathcal{J}_{y_{out}}$, $\mathcal{J}_{z_{in}} = \mathcal{J}_{z_{out}}$.

$$\begin{aligned} & m_1 v_{x_{1,in}} + m_2 v_{x_{2,in}} + \rho_* \frac{k_1}{2} y_{1,in} + \rho_* \frac{k_2}{2} y_{2,in} \\ & \quad = m_1 v_{x_{1,out}} + m_2 v_{x_{2,out}} + \rho_* \frac{k_1}{2} y_{1,out} + \rho_* \frac{k_2}{2} y_{2,out} \end{aligned} \tag{4.24}$$

$$\begin{aligned} & m_1 v_{y_{1,in}} + m_2 v_{y_{2,in}} - \rho_* \frac{k_1}{2} x_{1,in} - \rho_* \frac{k_2}{2} x_{2,in} \\ & \quad = m_1 v_{y_{1,out}} + m_2 v_{y_{2,out}} - \rho_* \frac{k_1}{2} x_{1,out} - \rho_* \frac{k_2}{2} x_{2,out} \end{aligned} \tag{4.25}$$

$$\begin{aligned} & m_1 x_{1,in} v_{y_{1,in}} - m_1 y_{1,in} v_{x_{1,in}} + m_2 x_{2,in} v_{y_{2,in}} - m_2 y_{2,in} v_{x_{2,in}} \\ & \quad - \rho_* \frac{k_1}{2} \left(x_{1,in}\right)^2 - \rho_* \frac{k_1}{2} \left(y_{1,in}\right)^2 \rho_* - \rho_* \frac{k_2}{2} \left(x_{2,in}\right)^2 - \rho_* \frac{k_2}{2} \left(y_{2,in}\right)^2 \\ & \quad = m_1 x_{1,out} v_{y_{1,out}} - m_1 y_{1,out} v_{x_{1,out}} + m_2 x_{2,out} v_{y_{2,out}} - m_2 y_{2,out} v_{x_{2,out}} \\ & \quad - \rho_* \frac{k_1}{2} \left(x_{1,out}\right)^2 - \rho_* \frac{k_1}{2} \left(y_{1,out}\right)^2 \rho_* - \rho_* \frac{k_2}{2} \left(x_{2,out}\right)^2 - \rho_* \frac{k_2}{2} \left(y_{2,out}\right)^2 \end{aligned} \tag{4.26}$$

Moreover the same relations can be deducted by means of the asymptotic equations (4.7). In the following chapter this novel method will be tested analytically in the perfectly symmetrical scattering, while a numerical check will be provided in more complicated scenarios where new physical effects arise.

Chapter 5

Simulations of the VA-scattering

"I... a universe of atoms, an atom in the universe."

Richard P. Feynman

Vortices are present in a broad range of phenomena in physics, from quantum optics, to superconductors [7] and Josephson-junction arrays, but the most representative and controllable environments are represented by ultracold quantum gases [11] and superfluids [9]. The experimental realization of Bose-Einstein Condensation by means of laser cooling and evaporating cooling techniques in rubidium, sodium and potassium atoms opened a vast number of theoretical and experimental challenges. After many experiments, quantized vortices have been observed in superfluid ^{2}He, extremely close to the ideal frictionless fluid, and subsequently in superfluid ^{4}He. Moreover the detection of vortices in ultracold bosons (BECs) shed a light on a new vast phenomenology to explore leading to experiments containing rotating condensates and many technological employments.

The introduction of the Point-like model in scientific literature permitted to focus the attention on the dynamical features of quantum vortices, investigating their trajectories when trapped into circular boxes by means of harmonic potentials. Such analytical model has been validated by means of numerical comparisons [14] with the original mean-field dynamics arising from the Gross-Pitaevskii equation. Recent works suggested how the emergence of massive cores, occurring within boson mixtures, profoundly changes the dynamics playing the role of an non-rotating

inertial mass and resulting in a singly quantized vortex in one hyperfine component surrounding a core of the second component [6].

The system under investigation is then constituted by a pair of quantum vortices arising from a binary mixture of BECs. The mixture considered is made of Potassium ^{41}K, of mass $m_a = 1{,}42 * 10^{-25} kg$, and Rubidium ^{87}Rb, with approximate mass of $m_b = 6{,}48 * 10^{-26} kg$. The former will be addressed as the a-species, acting as a confining potential on the latter, the b-species, that plays the role of a non-rotating massive core. Being the vortex-antivortex dynamics (VA) the object of this work the two vortices have opposite charge (e.g. $k_1 = -k_2$) with counter-rotating angular velocities $\Omega = 5 rad/s$. Such dipole can be considered as a free particle of overall mass $M \approx 2m$ but close to a boundary (the border of the domain, a wall or an obstacle as in this case), the emergence of interaction effects drastically alter its dynamics.

In the following tractation various numerical simulations with an increasing level of complexity will be presented with the main purpose of approaching the most realistic experimental scenarios. In the first part basic physical settings will be investigated and compared with the main goal of emphasizing the main parameters guiding the transition from different dynamical behaviours. Trivial initial settings will be taken into account such as a 1-dimensional velocity field direct to the obstacle, the influence of the order of magnitude of initial velocities as well as other geometrical factors with the goal of exploring the phenomenology behind vortex scattering processes. In the subsequent discussion it will be introduced a 2-dimensional velocity field with different components, various inclinations of the dipole's axis but also mass unbalances will be examined in order to simulate realistic scenarios that are much more likely to occur in experimental setups.

5.1 The recombination of the pair

The first simulations explore the most basic scenario where the two vortices with equal masses are initially located symmetrically with respect to the $y - axis$ and at fixed distance from the obstacle, with non-zero initial velocity only along the vertical axis of value $v_{y_{in}} = 5 * 10^{-6} m/s$. It is interesting to note, despite the high non-linearity of the dynamical system, the overall appearing stability of such trajectories. The vortex-antivortex dipole seems to be a solid configuration that is just altered when the balance between attraction and repulsion forces between them is disrupted by the appereance of repulsion effects induced by the proximity to the obstacle. Indeed, the original dipole length is restored and the trajectories appears perfectly symmetrical with respect to the $y - axis$.

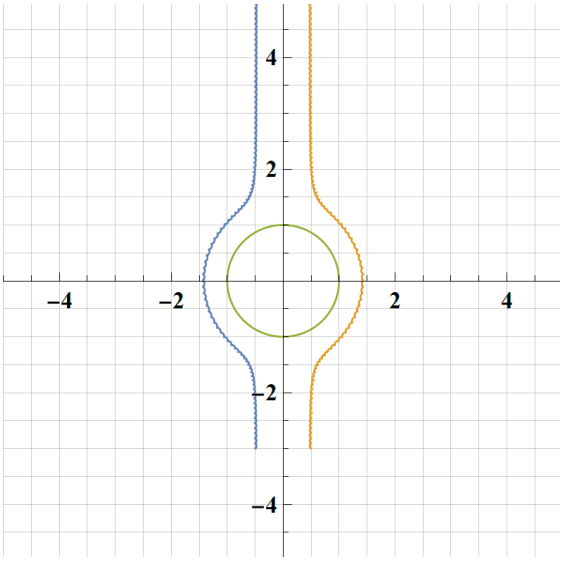

Figure 5.1: Perfectly symmetrical scattering when symmetrical initial conditions are imposed for both positions and velocities.

The same identical phenomenology is observed increasing the order of magnitude of the initial velocity: by imposing $v_{y_{in}} = 5 * 10^{-4} m/s$ it has been possible to notice once again the recombination of the pair at the original length despite the emergence of visible oscillations. In this regard the presence of a higher velocity field seems to induce dynamical instabilities responsible for the appearance of an oscillatory dynamics of the vortices. Indeed the equilibrium distance, when the equilibrium between attraction and repulsion forces between them is reached, seems to be no longer present and the dipole continuously expands and contracts like a spring subject to periodic forces.

Considering the most basic scenario where totally symmetrical initial conditions are imposed, the conservation of (4.21) provides specific relations between the initial velocities of the pair and their final velocities. Concerning the first generator $\mathcal{J}_{x_{in}} = \mathcal{J}_{x_{out}}$ gives, emphasizing that $k_1 = -k_2$:

$$\begin{aligned} m_1 v_{x_{1,in}} + m_2 v_{x_{2,in}} + \rho_* \frac{k_1}{2} y_{1,in} + \rho_* \frac{k_2}{2} y_{2,in} \\ = m_1 v_{x_{1,out}} + m_2 v_{x_{2,out}} + \rho_* \frac{k_1}{2} y_{1,out} + \rho_* \frac{k_2}{2} y_{2,out} \end{aligned} \tag{5.1}$$

where the imposition of null horizontal initial velocities for the vortices and the experimental observation that $v_{x_{1,out}} \approx v_{x_{2,out}} \approx 0$, as a consequence of the (almost) uniform motion along y, allow to prove the equivalence. For the the second

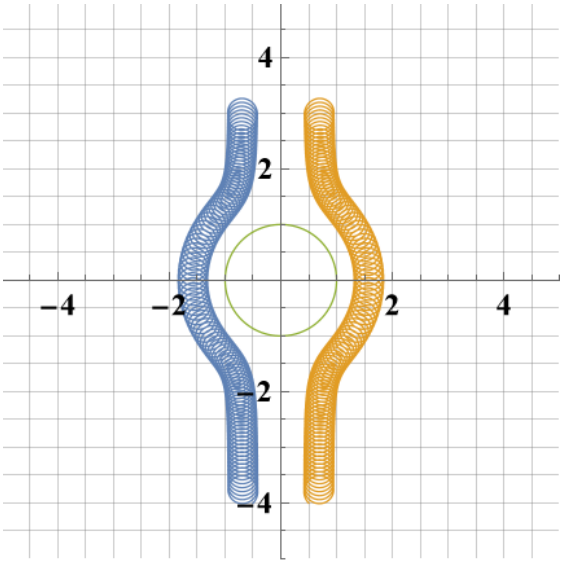

Figure 5.2: Velocity field has only y-component of $5 * 10^{-4}$ for both vortices. Increasing the velocity results in stimulating the oscillatory dynamics, despite the mean trajectories reflect the original set up.

generator instead $\mathcal{J}_{y_{in}} = \mathcal{J}_{y_{out}}$ gives:

$$\begin{aligned} m_1 v_{y_{1,in}} + m_2 v_{y_{2,in}} - \rho_* \frac{k_1}{2} x_{1,in} - \rho_* \frac{k_2}{2} x_{2,in} \\ = m_1 v_{y_{1,out}} + m_2 v_{y_{2,out}} - \rho_* \frac{k_1}{2} x_{1,out} - \rho_* \frac{k_2}{2} x_{2,out} \end{aligned} \tag{5.2}$$

that under the straightforward observation that $v_{y_{1,in}} = v_{y_{2,in}}$ and $v_{y_{1,out}} = v_{y_{2,out}}$, but also $x_{1,in} = x_{1,out}$ and $x_{2,in} = x_{2,out}$ due to the symmetry property of the observed dynamics, one finds that

$$v_{G,y,in} = v_{G,y,out}$$

The quantity $v_{G,y} = (v_{y_1} + v_{y_2})/2$ can be seen as the dipole's center of mass vertical velocity that, in the light of the resulting relation, appears to be conserved during the scattering process. For the last generator then, by imposing $\mathcal{J}_{z_{in}} = \mathcal{J}_{z_{out}}$ it is possible to obtain:

$$\begin{aligned} & m_1 x_{1,in} v_{y_{1,in}} - m_1 y_{1,in} v_{x_{1,in}} + m_2 x_{2,in} v_{y_{2,in}} - m_2 y_{2,in} v_{x_{2,in}} \\ & \quad - \rho_* \frac{k_1}{2} \left(x_{1,in}\right)^2 - \rho_* \frac{k_1}{2} \left(y_{1,in}\right)^2 \rho_* - \rho_* \frac{k_2}{2} \left(x_{2,in}\right)^2 - \rho_* \frac{k_2}{2} \left(y_{2,in}\right)^2 \\ & \quad = m_1 x_{1,out} v_{y_{1,out}} - m_1 y_{1,out} v_{x_{1,out}} + m_2 x_{2,out} v_{y_{2,out}} - m_2 y_{2,out} v_{x_{2,out}} \\ & \quad - \rho_* \frac{k_1}{2} \left(x_{1,out}\right)^2 - \rho_* \frac{k_1}{2} \left(y_{1,out}\right)^2 \rho_* - \rho_* \frac{k_2}{2} \left(x_{2,out}\right)^2 - \rho_* \frac{k_2}{2} \left(y_{2,out}\right)^2 \end{aligned} \tag{5.3}$$

which leads to the conservation law:

$$y_{1,in}^2 + y_{2,in}^2 = y_{1,out}^2 + y_{2,out}^2 \tag{5.4}$$

in the light of the fact that $x_{1,in} = -x_{2,in}$.

It is then possible to conclude that, in the perfectly symmetrical scattering process, the aforementioned approach based on the consideration of the *asymptotic regimes* provided reasonable and consistent results. Nevertheless satisfaction of aforementioned conservation laws has been verified numerically and provides satisfactory results.

As properly discussed in previous chapter, the existence of such dynamical subregimes in which the role of masses is negligible permits to restore the dynamics of massless vortices embodied by the Helmoltz-Kirchoff equations. To numerically validate such result, various comparisons has been conducted simulating massive vortices and their massless counterpart. As showed by following pictures, the agreement is extraordinary and overall the dynamics is equivalent except for the transient in which the highly non-linear interactions with the obstacle induce weak oscillations. This represents a further confirmation of the methodology introduced

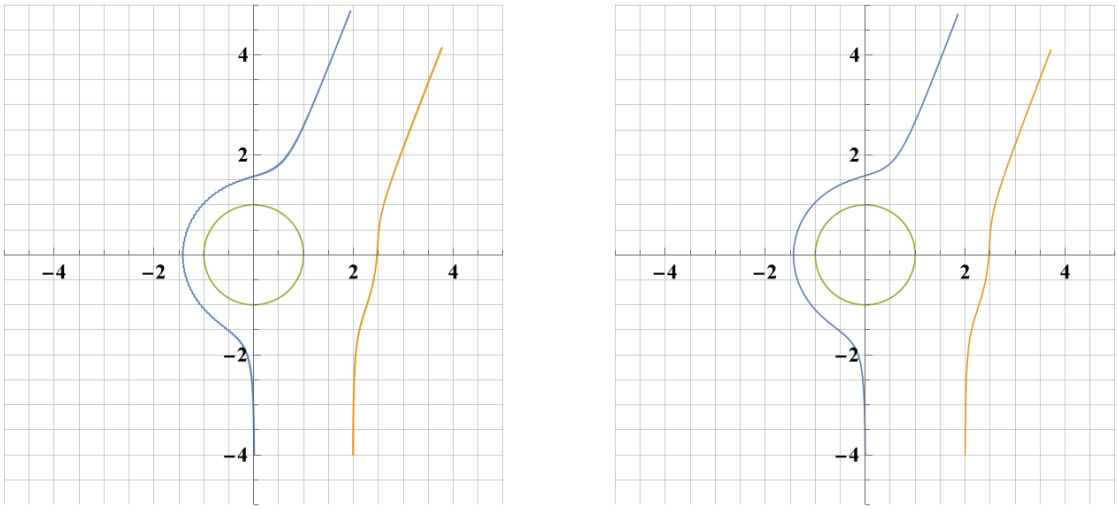

Figure 5.3: Comparison between massive (left) and massless dynamics (right) of the VA scattering. Simulations present identical initial conditions.

and especially a validation of the consequent statements concerning the role of the masses.

5.2 The emergence of the deflection angle

To explore the role of asymmetrical initial conditions, by keeping the elongation of the dipole fixed for the entire sequence of tests, its center of mass has been gradually shifted with respect to the center of the obstacle. What emerges is that it exist a critical positioning for the center of mass (approximately $x_{center} \in (1.75, 2.25)$) in which the dynamical behaviour drastically changes as a consequence of a phase transition. While for values smaller than 1.75 the dipole is stretched and one vortex encircles the obstacle, for $x_{center} \geq 2.25$ the pair remains compact and stable at fixed length. An interesting phenomena is the resulting curvature effect produced by the obstacle on the trajectories of the vortices.

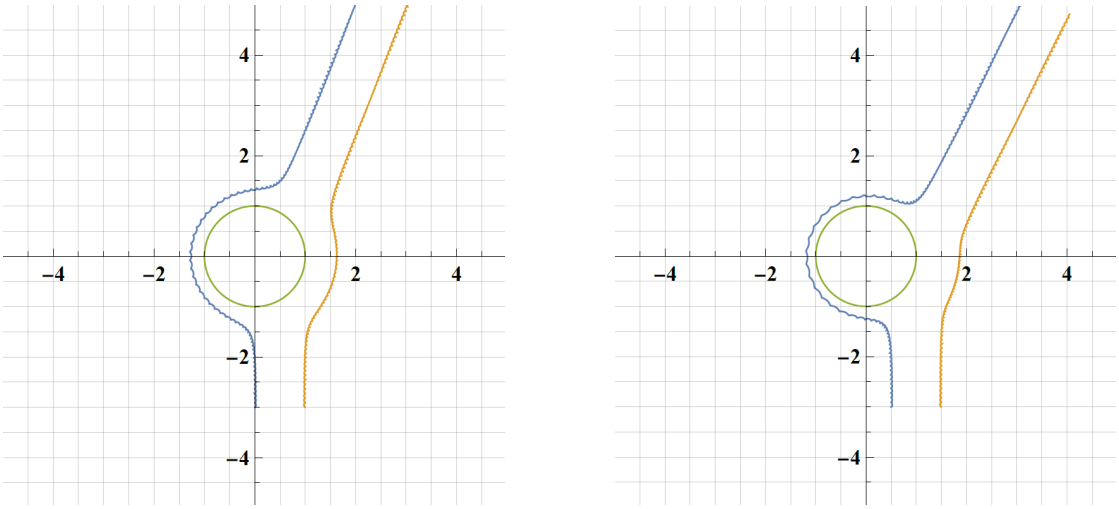

Figure 5.4: Velocity field has components identically null. In the left picture the center of mass of the dipole is positioned at $x_{bar} = 0{,}5 * R$ and at $x_{bar} = 1 * R$ in the right one.

An interesting phenomena is the *deflection angle* produced behind the obstacle: despite the two vortices recombine in a dipole with original length unaltered, their trajectories appears to be bent of a certain angle with respect to the $x-axis$.

As properly discussed in section 4.2.2, the asymptotic approach led to the discovery of conservation laws that have been verified analytically in the perfectly symmetrical scattering process. For the asymmetrical setting, the conservation of generators (4.21) has been verified numerically and the agreement is satisfactory.

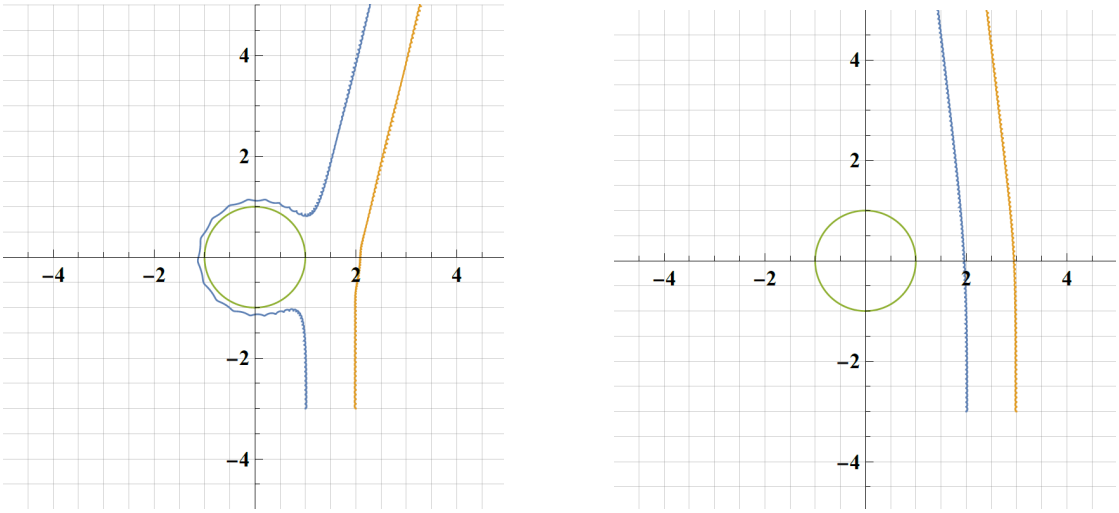

Figure 5.5: By keeping the dipole's length fixed, its center of mass is placed at $x_{bar} = 1{,}5 * R$ (left) and $x_{bar} = 2 * R$ (right). When x_{bar} is placed far enough, a visible qualitative change in the dynamics occurs.

5.2.1 The influence of geometric factors

Another relevant parameter altering the dynamical behaviour of the system is the elongation of the vortex dipole: changing the length of the pair results in altering the overall dynamical behaviour of the system. As can be seen in the following, the overall effect of decreasing such length is increasing the interaction effects between the components, leading to configurations where the the attraction to its corresponding anti-vortex is much greater than the repulsion induced by the obstacle to the left vortex (in blue). Although it would be reasonable to assume that in virtue of the proximity of the vortices their mutual interactions should be stronger than the influence of the boundary, resulting in keeping the dipole much more compact and less likely to stretch, simulations showed multiple numerical errors for a wide range of positionings. Resulting plots showed how, close to the boundary, the trajectories started to split in order to surround it but somehow end up too close to it that the strong repulsion forces resulted in pushing the vortices far away in the plane region. This phenomena occurs for $x_{center} \in (0.5, 1.5)$, the region in which a dynamical phase transition occurs separating the two different behaviours: the bypassing on one hand and the deflection on the other. So despite a slight, moderate shift produces a deflection angle analogue to the one discussed in the previous section, when the dipole is too tight vast numerical errors appear and a drastic transition between two behaviour is present. Moreover the closedness of the vortices results in the visible emergence of ripples in their trajectories as a consequence of the constant competition between attraction and repulsion forces between them.

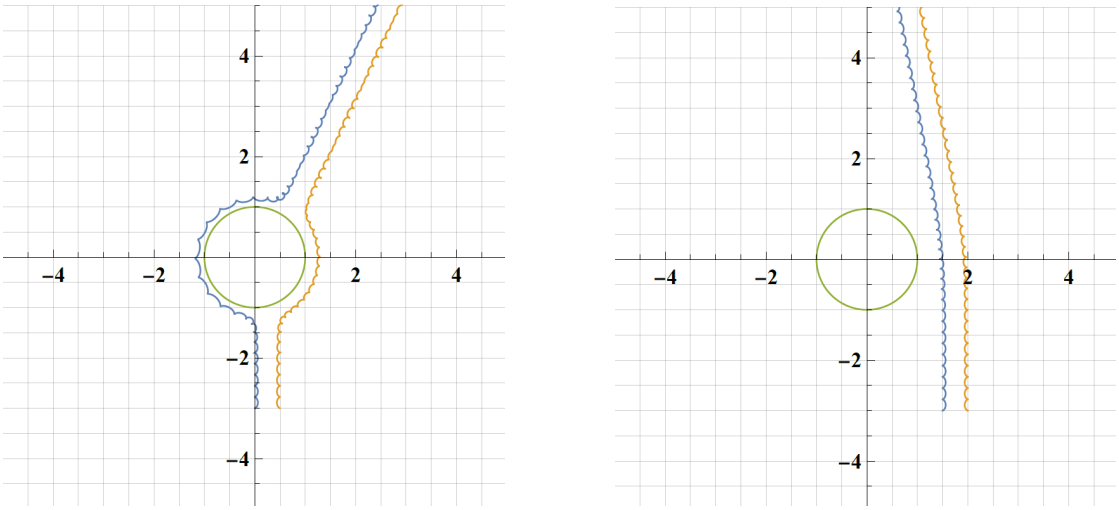

Figure 5.6: The transition from capture to deflection occurs much sooner as a consequence of the reduced initial distance between the vortices (here fixed at $d = 0{,}5 * R$). Moreover a stronger oscillatory pattern arises due to the stronger interactions between the dipole's components.

From this first set of physical settings what emerges is the surprisingly stability and compactness of the VA-pair when colliding against a smooth obstacle. The emergence of perfectly symmetrical trajectories, aside from ripples of variable magnitude, is a reasonably unexpected result considering the high degree of complexity of the dynamical equation. Moreover a deep influence of the relative positioning of the dipole with respect to the obstacle and the mutual distance between the vortices arised. On one hand, by keeping the dipole's length fixed and shifting its center of mass, a visible deflection angle appears after the pair recombines. On the other, a stable, safe distance seems to be able to avoid critical phenomena and guarantee (almost) smooth orbits.

5.3 Experimental Scenarios

Since a large gas of vortices depicts a scenario with many possible configurations, trivial settings with identical velocity components or masses are rare in experimental situations. In order to explore more realistic experimental set ups it will now be considered more complex settings that are much more likely to occur.

5.3.1 Inclined axis

Another geometrical parameter guiding the transition from the two distinct regimes (capture and deflection) is the *inclination* of the dipole's axis. In the present section, by keeping the vortex's position fixed (blue), the antivortex (orange) will be located at the same, constant distance but appropriately positioned in order to produce slightly increasing angles.

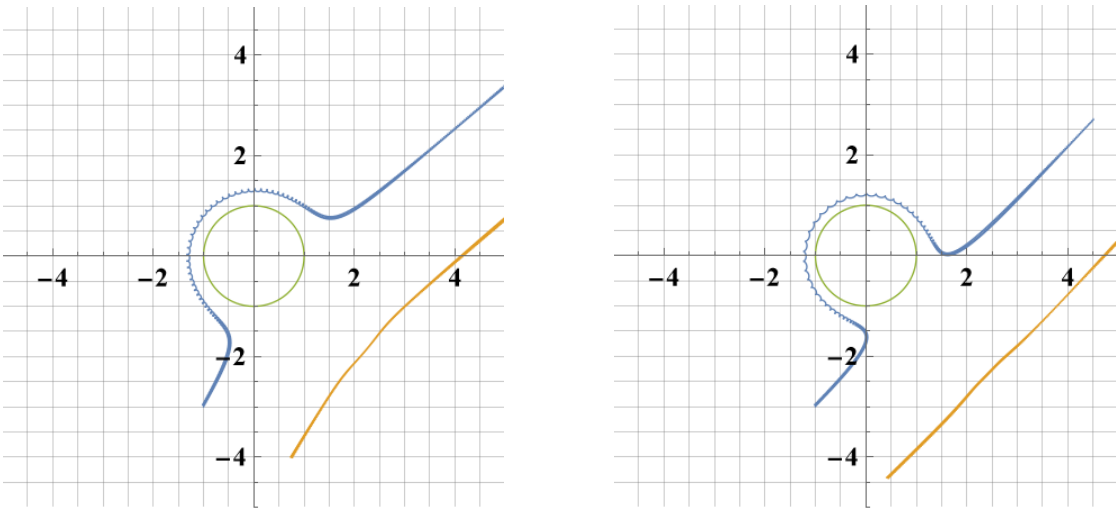

Figure 5.7: Initial velocity field has components $\vec{v_1} = \vec{v_2} = (5 * 10^{-5} m/s; 5 * 10^{-5} m/s)$; the dipole is inclined of 30 (left) and of 45 (right) with respect to the x-axis.

Figure 5.7 shows how for angles $\alpha \in [0, 45)$ the dipole is still subject to a transient elongation, while surrounding the disk, followed by the usual recombination. Conversely, for higher inclinations ($\alpha \geq 60$) the situation changes and the dipole preserves its length while bending the trajectory of its center of mass as a result of the interaction induced by the obstacle.

5.3.2 The influence of velocity differences

To investigate the role of asymmetrical initial velocities, in the first round of simulations it will be taken into account the case of a velocity field directed along the y-axis for one vortex, while the other is initially stationary. Simulations show how despite initial positions are symmetrical, the trajectories recombine along an inclined axis. The introduction of unbalances in initial velocities then produces an asymmetrical scattering also presenting wider oscillations compared to the analogue setting with equal velocities. Moreover such oscillatory behaviour appears to be asynchronous, meaning that when the oscillation amplitude of one vortex

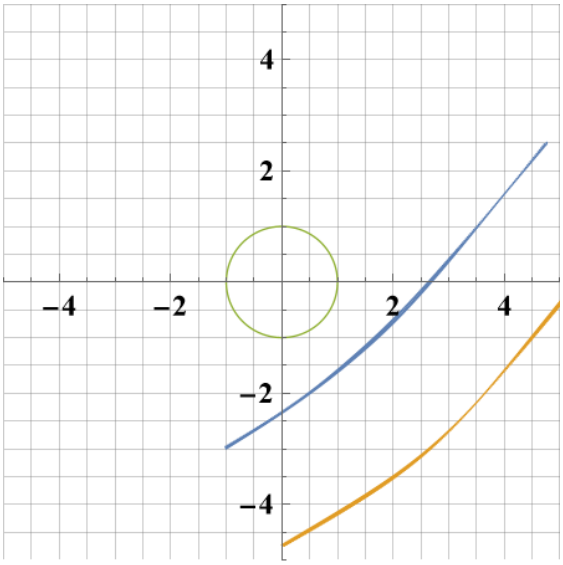

Figure 5.8: Initial velocity field has components $\vec{v_1} = \vec{v_2} = (5 * 10^{-5} m/s, 5 * 10^{-5} m/s)$; the dipole is inclined of 60 with respect to the x-axis. This setting shows the passage from the capturing dynamics to the deflection of the vortices' trajectories.

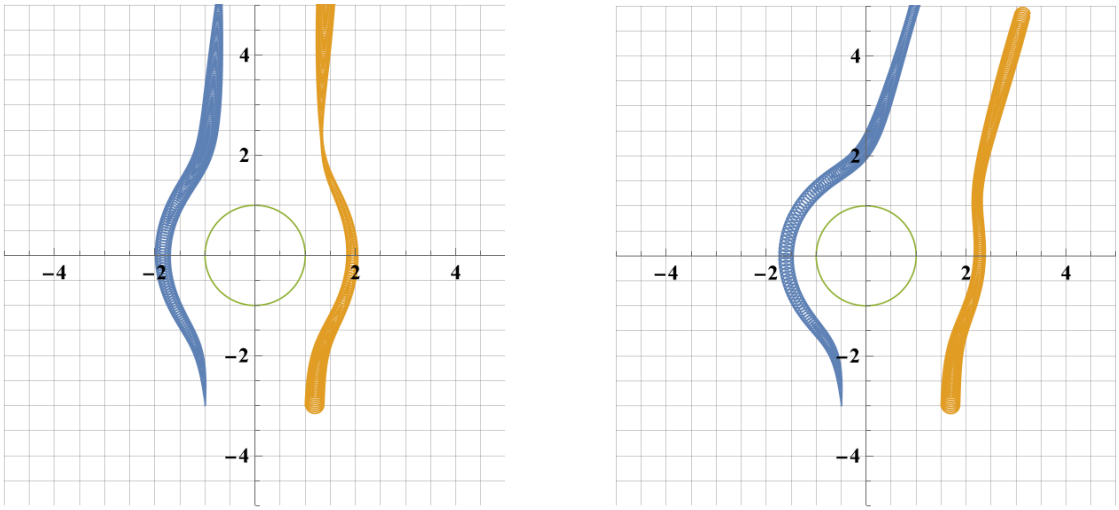

Figure 5.9: Perfectly symmetrical scattering with $\vec{v_1} = (0; 0)$, $\vec{v_2} = (0; 5 * 10^{-4} m/s)$ (left); while x_{bar} is slightly shifted (right). Both simulations are consistent with original scenarios, aside from wider oscillations with an apparent asynchronous behaviour.

reaches its maximum, the other vortex is close to its minimum oscllatory behaviour.

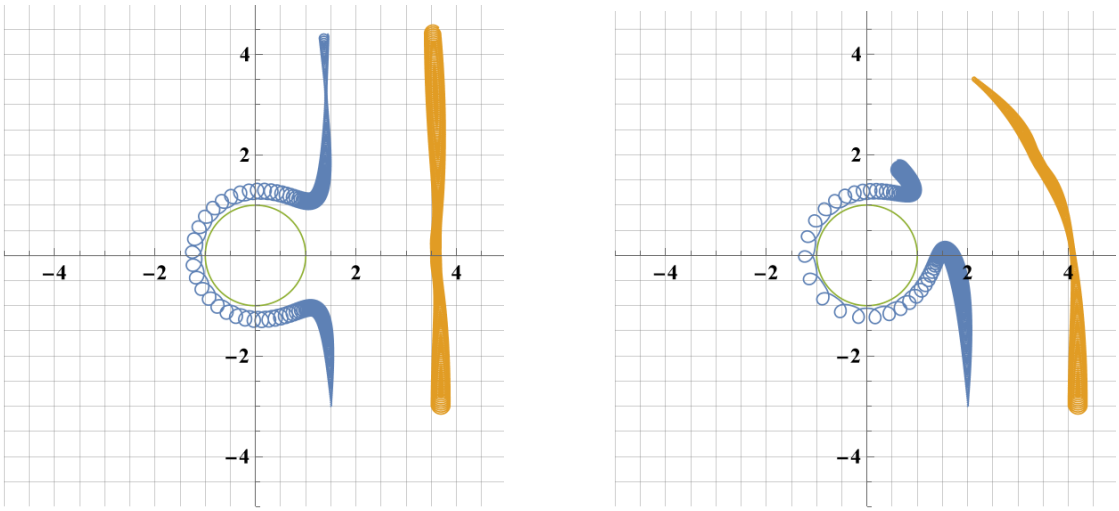

Figure 5.10: Contrary to the case of equivalent velocities, the region in which the capture occurs is much wider. Velocity fields are still set as $\vec{v_1} = (0; 0)$, $\vec{v_2} = (0; 5 * 10^{-4} m/s)$.

Another interesting result concerns figure 5.10, showing that in a few scenarios the introduction of destabilizing features may support the pair recombination. Indeed the setting depicted in right panel was already explored with completely symmetrical initial conditions and showed the occurrence of various numerical errors. The latter are a consequence of the fact that $x_{bar} = 3$ lays in the crossing region between the capture and the deflection behaviours, where the excessive closeness of left vortex (blue) to the disk produces significant repulsion effects able to push the vortex away and disrupting the dipole's structure. While infact for $x_{bar} < 3$ one observes the capture by the obstacle, for values greater than the critical one the deflection of the pair's trajectories occurs.

5.3.3 The influence of mass unbalances

This series of simulations is meant to explore mass-induced instabilities, by varying the core's mass of one vortex and investigating the scattering properties of the resulting dipole, with the initial velocity fields kept fixed at $\vec{v_1} = (0; 5 * 10^{-5} m/s)$, $\vec{v_2} = (0; 5 * 10^{-5} m/s)$. Recalling that we indicated as species A the one laying in the vortex core and species B the one trapped into the other, for the former has been considered ^{87}Rb and ^{41}K for the latter, consistently with experimental

settings. Species A possess an approximate mass of $1{,}42 * 10^{-25} kg$, while the B species $6{,}48 * 10^{-26} kg$.

The greater kinetic contribution is intuitively embodied by the mass located in the vortex core, meaning that reducing of one order of magnitude the mass of B species (the massive core) is not expected to produce significant differences in the system's dynamics. Numerical simulations strongly confirm this guess, suggesting

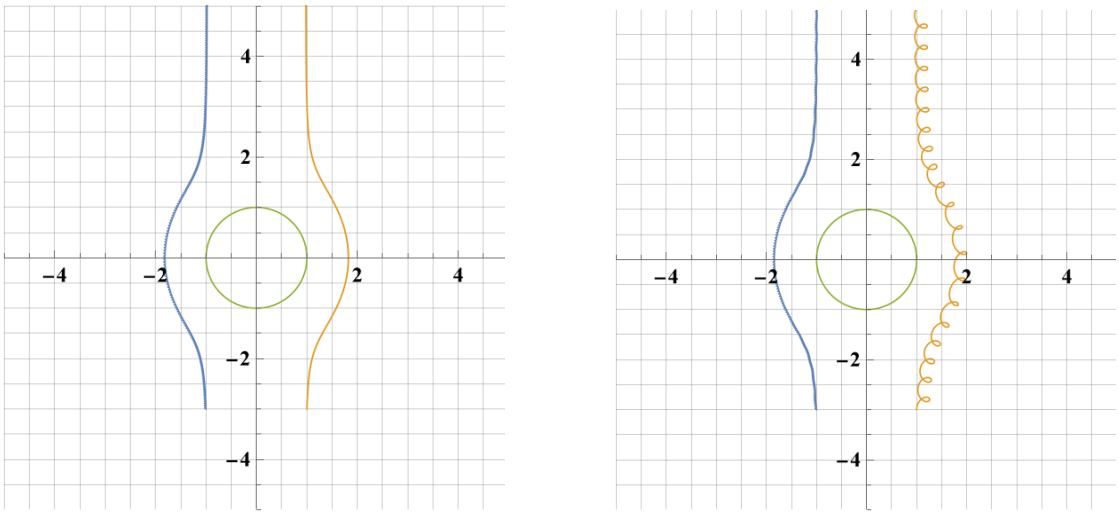

Figure 5.11: Reducing the core's masses of one order of magnitude doesn't produce visible effects (left), while increasing it provides the emergence of ripples in the trajectory of heavier vortex (right)

that mass-induced instabilities may arise only when the kinetic contribution of the core becomes significant, possibly overtaking the one of species A. For this reason, only the increase of m_b of one and also two orders of magnitude depicts interesting and reasonable patterns. To explore the effects of such oscillations in the scattering dynamics without them being a driving factor, the core's mass has been maintained at $6{,}48 * 10^{-25} kg$ (only one order greater than the one employed in experiments) with the main goal of exploring combined effects of mass unbalances and geometrical factors.

As can be noticed by following pictures, such combination produces a noticeable increase in the oscillatory behaviour of the system: When the y-component velocity of lighter vortex its oscillations get wider and a slight deflection angle in left direction appears. Contrary, when heavier vortex possesses a non-zero velocity along y-axis its oscillatory behaviour drastically increases and a slight deflection angle in right direction can be noticed. This suggest that counterintuitively, aside

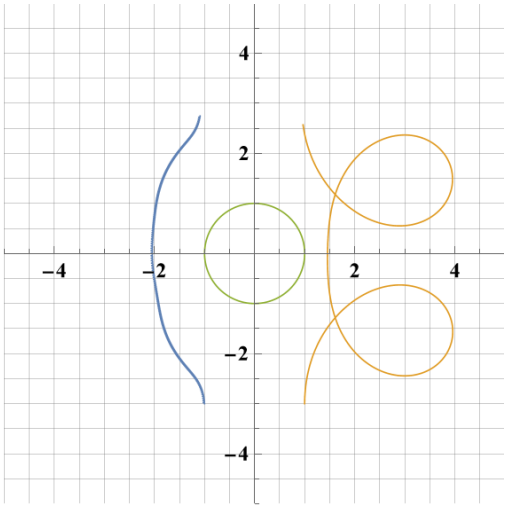

Figure 5.12: With two orders bigger, the mass of vortex 2 (orange) produces remarkable ripples in its trajectory.

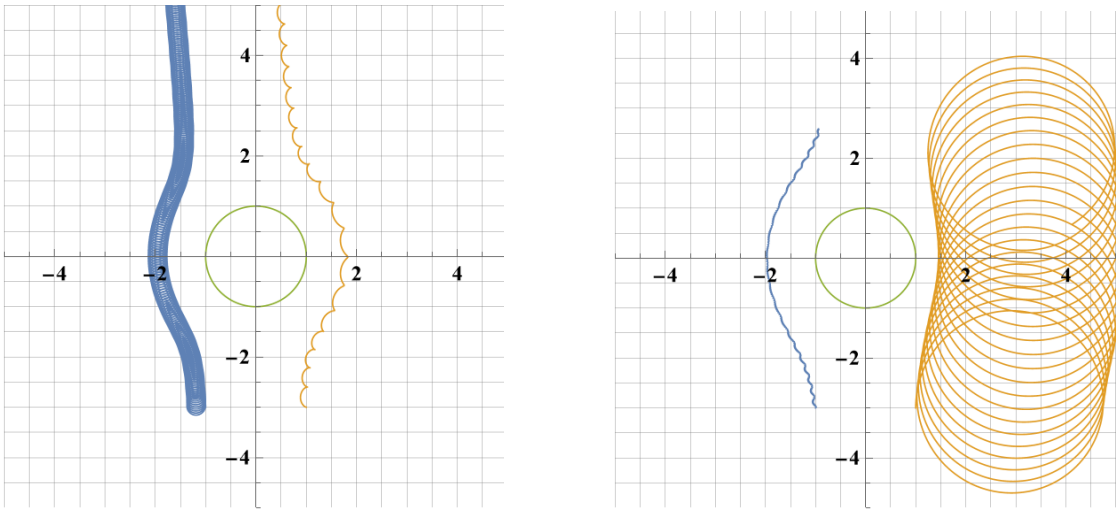

Figure 5.13: An increase of the y-component velocity of one vortex further increase the amplitude of oscillations. For left panel $\vec{v_1} = (0; 5{*}10^{-4} m/s)$, $\vec{v_2} = (0; 0)$, while $\vec{v_1} = (0; 0)$, $\vec{v_2} = (0; 5 * 10^{-4} m/s)$ for the right one.

from the emergence of strong oscillations, the presence of mass unbalances, thus shifting the center of mass of the dipole, is not directly correlated with an asymmetrical scattering. The emerge of a deflection angle (so the recombination along an inclined axis) arises when a consistent difference bewteen velocity profiles is introduced.

5.4 The case of VV-scattering

Despite the main focus of this work has been the investigation of the dynamics of the vortex-antivortex pair, a few experimental settings involving vortex-vortex dipoles have been explored for the sake of curiosity. Despite their limited employment in physical applications, it turned out that VV-dipoles can express a much more complex and fascinating dynamics, presumably as a consequence of the superposition of the two vorticity fields possessing equal sign. Indeed the main hypotesis is that the accumulation of vorticity may be an instability feature for the system that breaks the ordered motion previously observed for the VA-pair.

Despite the pattern is much more exotic than the VA scattering case, the dynamics still doesn't appear to be *chaotic*. Indeed the system doesn't seem to be sensible to initial conditions as a regular overall motion can be observed despite the higher complexity. If observed for longer times, trajectories don't close resulting in an *aperiodic motion* that is the combination of a precession of the two vortices around their center of mass with a rotation of the latter around the disk-like obstruction. Nevertheless the introduction of non-zero velocity components

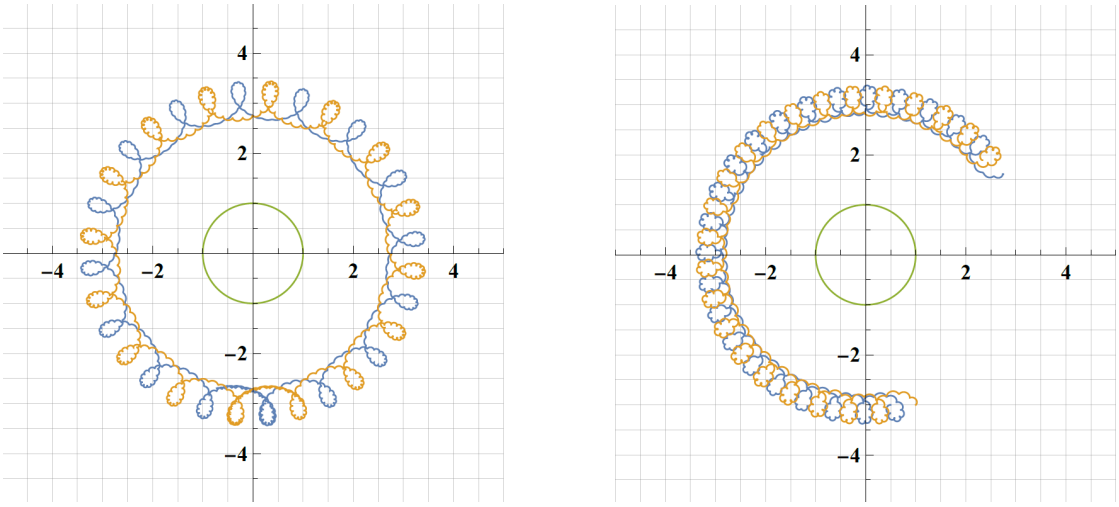

Figure 5.14: Velocity field is identically null for both vortices and $k_1 = -k_2$. The overall dynamics is drastically different from the VA case as a consequence of an accumulation of local vorticity.

in the simulation specifics easily alters the observable pattern as shown by figure 5.15, despite the superposition of the aforementioned combined motions can be noticed. When the two vortices are initially placed on opposite sides of the disk a surprising phenomenon has been observed, seeing the two vortices co-rotating around the obstacle on the same orbit.

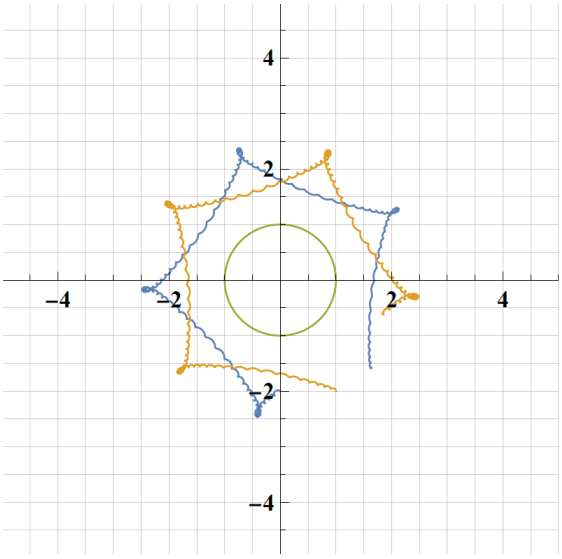

Figure 5.15: Initial velocity field has components $\vec{v_1} = \vec{v_2} = (5 * 10^{-6}; 0)$ and $k_1 = -k_2$

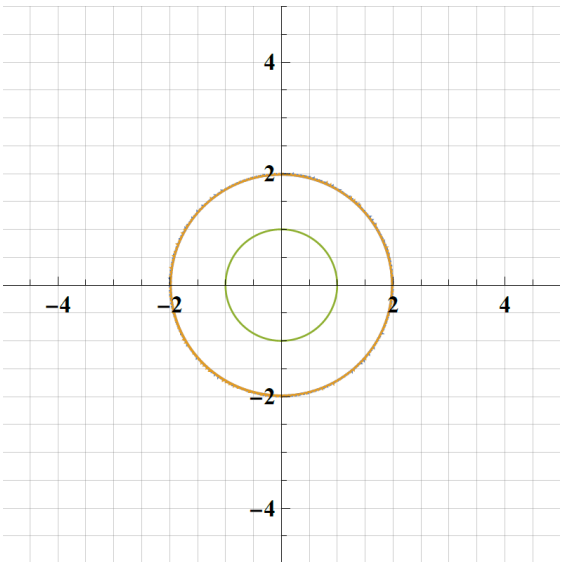

Figure 5.16: Vortices are initially located symmetrically above and below the obstacle, with initial velocity fields $\vec{v_1} = \vec{v_2} = (0; 5 * 10^{-6})$

Chapter 6

Conclusions and Further Developments

The present work has been devoted to the investigation of vortex-antivortex (VA) scattering against a disk-like obstacle with the main purpose of discovering and characterizing its phenomenology. Assuming the existence of two asymptotic regimes where the influence of the obstacle proved to be reasonable and functioning. One the one hand it led to acquire translational symmetries, that were lost in proximity of the disk, and its corresponding conserved quantities able to provide a formula for the observed deflection angle behind the obstacle. On the other is gave a much more important result, stating that such asymptotic regimes are identified by the restoration of Helmoltz-Kirchoff equations describing massless vortices. As observed from numerical observation indeed, far from the influence of the obstacle the dipole appears to be moving in a uniform motion where acceleration components are negligible.

From the analytical viewpoint it has been necessary the implementation of a perturbative expansion of dynamical equations with the main purpose of separating zero-order contributions from first-order corrections. While the former, representing the bulk dynamics, resemble equations for massless vortices, the latter obey an ODE with linear dependence on perturbations and describe the oscillatory component of the observed trajectories. Further studies may rely on the investigation of the stability character of such trajectories in order to comprehend the eventual occurrence of chaos as the present study didn't notice any. Moreover the expansion of presented methodology may produce other important relations able to connect initial and final configurations of the system with the main purpose of characterizing the emergence of a rotation of the dipole's axis after interacting with the disk.

A broad number of simulations emphasized the influence of many parameters in such complex dynamics: from the elongation of the dipole to the centering with respect to the obstacle and also the inclination of the dipole's axis when approaching the obstacle. A considerable amount of experimental settings have been explored, starting from the most trivial ones and reaching a satisfactory level of complexity, all emphasizing the influence of many geometrical and dynamical parameters. The capture phenomenon have been observed with many different scenarios and in this regard the dipole proved to be remarkably stable despite the highly non-linear interactions with the obstacle. Indeed, the possibility to uncouple the zero-order dynamics to the first-order correction proved the existence of an "average" dynamics that is substantially stable. Such stable feature stands even when mass unbalances or asymmetrical velocities are introduced, aside from an eventual stimulation of the oscillatory character. Despite an appreciable ensemble of settings has been considered, many other parameters influencing the scattering dynamics are yet to be discovered, possibly leading to the emergence of new phenomenologies.

Quantum vortices are key in understanding various quantum mechanical systems and have a broad range of practical implications in quantum technology, superconductor design, plasma physics and quantum optics [14], [15], [7], [10]. The journey in understanding their complex phenomenology and non-linear interaction dynamics is long, harsh and full of mysteries. Many different approaches and points of view are necessary to properly investigate such complex physics and this work has the willingness of being a glimpse of one of the many.

Appendix A

Field Theory and Second Quantization

Within classical mechanics mathematicians and physicists developed a series of tools, addressed under the name of *Field Theory* [17], that permit to describe an almost infinite number of different problems arising in physics. Within its classical picture a field is a multivalued function of space and time that describes some physical entity of interest like position, velocity and vorticity but also electric and magnetic fields, or the quantum wavefunction. Field theory admits two perfectly equivalent pictures, a first one based on the introduction of a *Lagrangian* L and a second formulation relying instead on the development of an *Hamiltonian* $\mathcal{H}$. The link between the two representations is embodied by a Legendre transformation through which is defined the concept of *momenta*.

The former approach relies on the Lagrangian, defined as $L(q_i(t), \dot{q}_i(t), t) \doteq \mathcal{K} - \mathcal{U}$ the difference between kinetic and potential energy. In this framework the independent variables are represented by $q_i, \dot{q}_i, \quad i \in [1, n]$, generalized positions and velocities in configuration space, where n is the number of independent quantities representing also the system's *degrees of freedom*. The **action**, defined as the line integral of the Lagrangian along some curve γ in configuration space between two points, is formally expressed as a functional

$$\mathcal{S}[q; t_1, t_2] \doteq \int_{(\gamma)t_1}^{t_2} L\big(q(t), \dot{q}(t), t\big) dt \tag{A.1}$$

where t_1 and t_2 indicate the instants of the initial and final configuration of the system. Hamilton's principle of **stationary action** allows to deduce, from the

action functional, suitable dynamical equations:

$$\delta\mathcal{S} = 0 \Rightarrow \frac{\partial L}{\partial q_i} - \frac{d}{dt}\frac{\partial L}{\partial \dot{q}_i} = 0, \quad \forall i = 1, ..., n \tag{A.2}$$

known as **Euler-Lagrange equations**.

Conversely in Hamilton's picture of mechanics, dynamics is described by canonical variables $q_i, p_j, \quad i, j \in [1, n]$ representing generalized coordinates of phase space $\mathcal{P}$ and obeying usual Poisson Brackets

$$\{A.B\} = \sum_{i=1}^{n} \left(\frac{\partial A}{\partial q_i}\frac{\partial B}{\partial p_i} - \frac{\partial A}{\partial p_i}\frac{\partial B}{\partial q_i} \right), \quad \forall A, B \in F(\mathcal{P}) \tag{A.3}$$

which in present case give $\{q_i, p_j\} = \delta_{ij}$. The dynamical generator of the system is embodied by the Hamiltonian $\mathcal{H}$ defined as:

$$\mathcal{H}(q_i, p_j) = \sum_i p_i \dot{q}_i - L(q_i.\dot{q}_i) \tag{A.4}$$

where, as previously mentioned, the connection with Lagrangian formalism is addressed by a Legendre transformation defining the *canonical momenta*: $p_i \doteq \partial L/\partial \dot{q}_i$. **Hamilton's equations** are:

$$\dot{q}_i = \frac{\partial \mathcal{H}}{\partial p_i}, \quad \dot{p}_i = -\frac{\partial \mathcal{H}}{\partial q_i} \tag{A.5}$$

Within this formulation of mechanics, conserved quantities are found through canonical PB by means of the following argument: consider a generic function $A = A(q_i, p_l)$, its time derivative is calculated as

$$\frac{dA}{dt} = \sum_i \left(\frac{\partial A}{\partial q_i}\dot{q}_i + \frac{\partial A}{\partial p_l}\dot{p}_l \right) = \sum_i \left(\frac{\partial A}{\partial q_i}\frac{\partial \mathcal{H}}{\partial p_i} - \frac{\partial A}{\partial p_l}\frac{\partial \mathcal{H}}{\partial q_i} \right) \doteq \{A, \mathcal{H}\} \tag{A.6}$$

where Hamilton's equations have been employed. Thus it comes clear how, in order for quantity A to be conserved, it is necessary that condition $\{A, \mathcal{H}\}$ gets satisfied. This formalism is convenient when incorporating the second quantization process, employed anytime a quantum phenomena concerning many-body systems is investigated.

While the first quantization process prescribes the replacement of the canonical variables and Poisson Brackets with operators and commutators, the **second quantization** involves the quantization of the wavefunction ϕ viewed as a field involving normal modes. In particular, the starting point is the expression of the

wavefunction in terms of a linear combination of (time-independent) orthonormal vectors ϕ_l forming a basis $\mathcal{B} = \{\phi_l\}$ of a Hilbert space. Thus $\phi = \sum_l a_l(t)\phi_l(t)$ where a_l can be interpreted as the *normal modes* of the wavefunction; canonical Poisson Brackets are then exploited depending on canonical variables a_l:

$$\{A, B\} = \sum_l \left[\frac{\partial A}{\partial a_l}\frac{\partial B}{\partial a_l^*} - \frac{\partial A}{\partial a_l^*}\frac{\partial B}{\partial a_l}\right] \tag{A.7}$$

where $\{a_i, a_m^*\} = \delta_{im}/i\hbar$. The second quantization scheme provides an explicit way to replace such PB with commutators by substituting normal modes a_m^*, a_i with operators $b_m^\dagger$, b_i giving: $[b_i, b_m^\dagger] = \delta_{im}$ in parallel with the expression of the quantized field $\hat{\phi}(q,t) = \sum_l b_l(t)\phi_l(t)$.

Owing to its operator character, $\hat{\phi}$ fulfills the commutator $[\hat{\phi}(q,t), \hat{\phi}^\dagger(s,t)] = \delta^n(q-s)$ representing the commutator of a bosonic field within Quantum Field Theory. The **algebraic description** of bosonic-field commutators is then completed with commutators featuring the total number operator $\hat{N}$:

$$[\hat{\phi}(q,t), \hat{N}] = \hat{\phi}(q,t) \tag{A.8}$$

$$[\hat{\phi}^\dagger(q,t), \hat{N}] = -\hat{\phi}^\dagger(q,t) \tag{A.9}$$

Such canonical quantization is performed within an Hamiltonian formalism as follows. Consider a Lagrangian of the form

$$\mathcal{L} = \mathcal{L}\big(\phi_\alpha, \dot{\phi_\alpha}\big) = \int d^3x L\big(\phi_\alpha, \partial_i\phi_\alpha, \dot{\phi_\alpha}\big) \tag{A.10}$$

and introduce *momentum-like fields* π_α as canonically conjugate to ϕ_α defined as:

$$\pi_\alpha(y,t) \doteq \frac{\delta\mathcal{L}}{\delta\dot{\phi_\alpha}(y,t)} = \frac{\partial L}{\partial\dot{\phi_\alpha}(y,t)} \tag{A.11}$$

leading to express the field Hamiltonian as follows:

$$\mathcal{H}\big(\pi_\alpha, \phi_\alpha\big) = \sum_\alpha \int d^3y\big[\pi_\alpha(y,t)\dot{\phi_\alpha}(y,t) - L(\phi_\alpha, \dot{\phi_\alpha})\big] = \int d^3y H\big(\pi_\alpha, \phi_\alpha\big) \tag{A.12}$$

where $H\big(\pi_\alpha, \phi_\alpha\big)$ embodies the Hamiltonian density. At this point the field-version of usual PB between two fields $\mathcal{A}$, $\mathcal{B}$ reads:

$$\{\mathcal{A}, \mathcal{B}\} = \int d^3y \sum_\alpha \left[\frac{\delta\mathcal{A}}{\delta\phi_\alpha(y,t)}\frac{\delta\mathcal{B}}{\delta\pi_\alpha(y,t)} - \frac{\delta\mathcal{A}}{\delta\pi_\alpha(y,t)}\frac{\delta\mathcal{B}}{\delta\phi_\alpha(y,t)}\right] \tag{A.13}$$

where for $\delta\mathcal{A}/\delta\phi_\alpha$ it is intended the *functional derivative* of field $\mathcal{A}$ with respect to field ϕ_α (intuitively $\delta\phi(x)/\delta\phi(y) = \delta^3(x-y)$). Thus our (field) canonical Poisson Brackets read:

$$\big\{\phi_\alpha(x,t), \pi_\beta(y,t)\big\} = \delta_{\alpha\beta}\delta^3(x-y), \quad \big\{\pi_\alpha(x,t), \pi_\beta(y,t)\big\} = \big\{\phi_\alpha(x,t), \phi_\beta(y,t)\big\} = 0 \tag{A.14}$$

As previously discussed, the second quantization process prescribes the replacement of (field) PB A.14 with (field) commutators of the form $\{.,.\} \mapsto i\hbar[.,.]$ together with $\phi_\alpha \mapsto \hat{\phi}_\alpha(x,t)$, $\pi_\beta \mapsto \hat{\pi}_\beta(x,t)$. For non-relativistic bosonic field theories it is possible to consider the following Hamiltonian

$$\mathcal{H} = \int d^2x \psi^\dagger(x,t) H_0(x) \psi(x,t) + \frac{1}{2}\int d^3x \int d^3s \psi^\dagger(x,t)\psi^\dagger(s,t)U(x,s)\psi(x,t)\psi(s,t) \tag{A.15}$$

depending on fields $\psi, \psi^\dagger$, with $U(x,s)$ a potential accounting for interactions between particles.

Appendix B

Symmetries and Noether's Theorem

The concept of **symmetry** [13] is central in both classical and quantum physics due to its profound connection with the emergence of conservation laws. A symmetry is a transformation that leaves the system invariant, meaning that the equation of motion, as a system of differential equations, have the same form in the new and old variables. Another way to interpret a symmetry is a transformation that leaves the Lagrangian invariant modulo an additional total derivative.

Consider a system with a finite degrees of freedom described by a Lagrangian $L(q, \dot{q}, t)$ function of the generalized coordinates $q_i, i = 1, ..., n$, its time derivatives $\dot{q}_i$ and time t. Applying an *invertible point transformation* of the form:

$$t' = t'(t), \quad q_i'(t) = q_i'(q, t)$$

the Lagrangian will now be a different function of the new coordinates: $L'(q_i', \dot{q_i}', t')$. Although Lagrangians and Actions in the two reference systems must be unaltered, being scalars under point transformations,

$$\mathcal{S}[q_i; t_1, t_2] = \mathcal{S}'[q_i'; t_1', t_2'], \quad L(q_i, \dot{q}_i, t) = L'(q_i', \dot{q_i}', t')$$

the crucial fact is that what changes is their *functional dependence* on their arguments: L' and $\mathcal{S}'$ seen as functionals depending on $q_i', \dot{q_i}', t'$.

The equations of motion in the new set of coordinates are directly derived from the Lagrangian L' by means of Euler-Lagrange equations, but they generally differ from the original ones. For such point transformation to be a **symmetry** it is required the equivalence between the equation of motions in the two reference

frames, implying that the functional dependence of L and L' on their respective arguments is the same, modulo and additional total derivative:

$$L(q_i', \dot{q_i}', t') = L(q_i, \dot{q_i}, t) + \frac{df}{dt} \Leftrightarrow \mathcal{S}[q_i'; t_1', t_2'] = \mathcal{S}[q_i; t_1, t_2]$$

Such transformations may be *continuous* or *discrete* giving rise to corresponding types of symmetries. The set of all symmetries of a dynamical system that can be composed and inverted forms a group, called the *Symmetry Group* of the system, where each element corresponds to a specific symmetry transformation. For continuous symmetries, the symmetry group is often a *Lie Group*, where the infinitesimal generators of these transformations form a *Lie Algebra*, encoding the structure of the symmetry transformations. The conserved quantities correspond to the generators of the symmetry transformations in the Lie Algebra.

A key result, connecting the concepts of *symmetry* and *conservation law* is embodied in **Noether's Theorem** stating that if the action of a dynamical system is *invariant* under a continuous group (non-singular) transformations of the generalized coordinates and time of the form

$$t' = t'(t), \quad q_i' = q_i'(q, t)$$

and if the equations of motions are satisfied, then the quantity

$$Q \doteq \sum_i \frac{\delta L}{\delta \dot{q}_i} \delta q_i + L \delta t$$

is *conserved*. Basically it states that for every *continuous symmetry* of the action of a physical system, there exists a corresponding *conserved quantity* Q called **Noether Charge**. Invariance under specific transformations implies the emergence of the associated conserved Noether Charges: if the system's Lagrangian does not explicitly depend on time, the system is said to possess **time translation symmetry**, leading to the conservation of energy. If the Lagrangian does not explicitly depend on a certain spatial coordinate, the corresponding momentum is conserved implying **space translation symmetry**, while whenever the Lagrangian is invariant under rotations, angular momentum is conserved and **rotational symmetry** is gained.

Acknowledgements

This journey has come to an end. After years of studying for preparing exams, now a different chapter of my life is about to begin where I (hopefully) will have the chance to study to feed my curiosity, to explore the unknown and follow my dreams. All the things I've accomplished, everything I've done and all the adversities I will have to face, have been and forever will be possible with the right people surrounding me, encouraging me and believing in me. Concerning my academical journey, my path in Applied Mathematics has been deeply influenced by a few people that I would like to thank.

First of all prof. Rondoni who constantly supported me and guided me during last year while searching for PhD positions. I am thrilled for these upcoming years as a PhD student under your supervision and glad for this incredible opportunity. Prof. Cortese, a mentor, an inspiration and an outstanding professor. My choice of pursuing Mathematics is all because of you and your lessons, your stories and your speeches, because of all the curiosity you have conveyed to me and for teaching me that beside every piece of Mathematics, behind every equation and every formula there is a human being worthy of being recognized, understood and appreciated.

Thanks to prof. Grillo, for the incredible source of knowledge, humour and passion but most importantly because thanks to you and your lessons I've had the courage to jump into Physics for this Master's project, pursuing a long-standing desire. Thanks to Alice Bellettini for all the precious advices concerning academia and for teaching me everything I needed to know in order to simulate those fascinating vortices.

But most importantly, thanks to my mentor and supervisor prof. Vittorio Penna. I would like to thank you with all my heart for all the lessons, the countless hours spent in your offices debating about vortices, for your unconditional support and for being an incredible guide during all this year of work. Your passion for your work and for Physics truly captured me in a way I couldn't describe, stimulating in me a pure desire to search, explore and discover.

References

[1] V. Penna A. Bellettini A. Richaud. "Relative dynamics of quantum vortices and massive cores in binary BECs". In: *The European Physics Journal Plus* 138 (2023).

[2] A. Fetter A. Richaud V. Penna. "Dynamics of massive point vortices in a binary mixture of Bose-Einstein condensates". In: *Physical Review A* 103 (2021).

[3] A. Fetter A. Richaud V. Penna. "Massive Quantum Vortices in Superfluids". In: *Journal of Physics: Conference Series* 2494 (2023).

[4] V. Penna A. Richaud. "Quantum dynamics of bosons in a two-ring ladder: Dynamical algebra, vortexlike excitations, and currents". In: *Physical Review A* 96 (2017).

[5] V. Arnold. *Metodi Matematici della Meccanica Classica*. Editori Riuniti, 1992.

[6] S. Bandyopadhyay, A. Roy, and D. Angom. "Dynamics of phase separation in two-species Bose-Einstein condensates with vortices". In: *Physical Review A* (2017).

[7] G. Blatter et al. "Vortices in high-temperature superconductors". In: *Review of Modern Physics* 66 (1994).

[8] N. G. Parker C. F. Barenghi. *A Primer on Quantum Fluids*. Springer, 2016.

[9] R. J. Donnelly. *Quantized vortices in Helium II*. Cambridge University Press, 1991.

[10] R. Fazio and H. Van Der Zant. "Quantum phase transitions and vortex dynamics in superconducting networks". In: *Physics Reports* 355 (2001).

[11] A. Fetter. "Rotating trapped Bose-Einstein condensates". In: *Review of Modern Physics* 81 (2009).

[12] A. Gallemì et al. "Magnetic defects in an imbalanced mixture of two Bose-Einstein condensates". In: *Physical Review A* 97 (2018).

[13] W. Greiner. *Classical Mechanics*. Springer, 2010.

[14] P. Kuopanportti et al. “Splitting of singly and doubly quantized composite vortices in two-component Bose-Einstein condensates”. In: *Physical Review A* 100 (2019).

[15] W. J. Kwon et al. “Sound emission and annihilations in a programmable quantum vortex collider”. In: *Nature* (2021).

[16] S. Stringari L. P. Pitaevskii. *Bose-Einstein Condensation*. Oxford Science Publications, 2003.

[17] H. Nastase. *Classical Field Theory*. Cambridge University Press, 2019.

[18] V. Penna. *Lecture Notes on Advanced Quantum Mechanics and Quantum Statistics*. Department of Science and Applied Technology, Turin Polytechnic, 2023.

[19] V. Penna. “Quantum dynamics of two-dimensional vortex pairs with arbitrary total vorticity”. In: *Physical Review B* 59 (1999).

[20] V. M. Pèrez-Garcìa et al. “Low Energy Excitations of a Bose-Einstein Condensate: A Time-Dependent Variational Analysis”. In: *Physical Review Letters* 77 (1996).

[21] A. Richaud et al. “Mass-driven vortex collisions in flat superfluids”. In: *Physical Review A* 107 (2023).

[22] A. Richaud et al. “Vortices with massive cores in a binary mixture of Bose-Einstein condensates”. In: *Physical Review A* 101 (2020).

[23] P. G. Saffman. *Vortex Dynamics*. Cambridge University Press, 1994.